Selective Open-channel Block of *Shaker* (Kv1) Potassium Channels by S-nitrosodithiothreitol (SNDTT)

MATHEW W. BROCK,[1,2] CHRIS MATHES,[1] and WILLIAM F. GILLY[1,2]

[1]Hopkins Marine Station, Department of Biological Sciences, and [2]Neurosciences Program, Stanford University, Pacific Grove, CA 93950

ABSTRACT Large quaternary ammonium (QA) ions block voltage-gated K^+ (Kv) channels by binding with a 1:1 stoichiometry in an aqueous cavity that is exposed to the cytoplasm only when channels are open. S-nitrosodithiothreitol (SNDTT; $ONSCH_2CH(OH)CH(OH)CH_2SNO$) produces qualitatively similar "open-channel block" in Kv channels despite a radically different structure. SNDTT is small, electrically neutral, and not very hydrophobic. In whole-cell voltage-clamped squid giant fiber lobe neurons, bath-applied SNDTT causes reversible time-dependent block of Kv channels, but not Na^+ or Ca^{2+} channels. Inactivation-removed *Shaker*B (ShBΔ) Kv1 channels expressed in HEK 293 cells are similarly blocked and were used to study further the action of SNDTT. Dose–response data are consistent with a scheme in which two SNDTT molecules bind sequentially to a single channel, with binding of the first being sufficient to produce block. The dissociation constant for the binding of the second SNDTT molecule (K_{d2} = 0.14 mM) is lower than that of the first molecule (K_{d1} = 0.67 mM), indicating cooperativity. The half-blocking concentration ($K_{1/2}$) is ~0.2 mM. Steady-state block by this electrically neutral compound has a voltage dependence (about -0.3 e_0) similar in magnitude but opposite in directionality to that reported for QA ions. Both nitrosyl groups on SNDTT (one on each sulfur atom) are required for block, but transfer of these reactive groups to channel cysteine residues is not involved. SNDTT undergoes a slow intramolecular reaction ($\tau \approx 770$ s) in which these NO groups are liberated, leading to spontaneous reversal of the SNDTT effect. Competition with internal tetraethylammonium indicates that bath-applied SNDTT crosses the cell membrane to act at an internal site, most likely within the channel cavity. Finally, SNDTT is remarkably selective for Kv1 channels. When individually expressed in HEK 293 cells, rat Kv1.1–1.6 display profound time-dependent block by SNDTT, an effect not seen for Kv2.1, 3.1b, or 4.2.

KEY WORDS: voltage-gated potassium channels • ion channel gating • quaternary ammonium compounds • inactivation • nitrosylation

INTRODUCTION

Inactivation of voltage-gated potassium (Kv)* channels by large organic cations was first described by Armstrong (1969, 1971), who observed that injection of long-chain TEA derivatives (see Fig. 1) into voltage-clamped squid giant axons causes an exponential decay of I_K during a strong depolarization. This decay follows a normal activation time course, suggesting that block by these quaternary ammonium (QA) ions occurs only after the channel activation gates have opened (i.e., "open-channel block"). Also in agreement with a gated access mechanism, bound QA ions inhibit closing of channel activation gates after repolarization by what was later termed a "foot-in-the-door" effect (Yeh and Armstrong, 1978). This effect can be overcome at very hyperpolarized potentials, where channels can apparently be forced to close with blocker still bound. Unbinding (or recovery) is very slow at these voltages, leading to the concept that QA ions can be trapped in an internal cavity located between the channel selectivity filter and activation gate. The interpretation of these results as summarized above has become fundamental to the field (for reviews see Armstrong, 1972; Yellen, 1998)

Open-channel block of Kv channels subsequently has been observed for a large number of QA ions (French and Shoukimas, 1981; Swenson, 1981; Choi et al., 1993; Malayev et al., 1995; Snyders and Yeola, 1995) and protonated tertiary amines (Snyders et al., 1992; Rampe et al., 1993b; DeCoursey, 1995; Valenzuela et al., 1995; Yang et al., 1995; Horrigan and Gilly, 1996). Structures for a number of these compounds are shown in Fig. 1. The permanently charged QA compounds are relatively membrane-impermeant, and are most effective when applied to the cytoplasmic side of the membrane. Exter-

The present address of C. Mathes is Axon Instruments, 1101 Chess Drive, Foster City, CA 94404.

Address correspondence to William F. Gilly, Hopkins Marine Station, Oceanview Boulevard, Pacific Grove, CA 93950. Fax: (831) 655-6220; E-mail: lignje@leland.stanford.edu

*Abbreviations used in this paper: B/O, ratio of blocked to open channels; f_B, fraction of channel blocked; I_{Ca}, calcium current; I_K, potassium current; I_{Na}, sodium current; Kv channels, voltage-gated potassium channels; QA, quaternary ammonium; ShB, *Drosophila Shaker*B potassium channel; SNAP, S-nitroso-*N*-acetylpenicillamine; SNDTT, S-nitrosodithiothreitol.

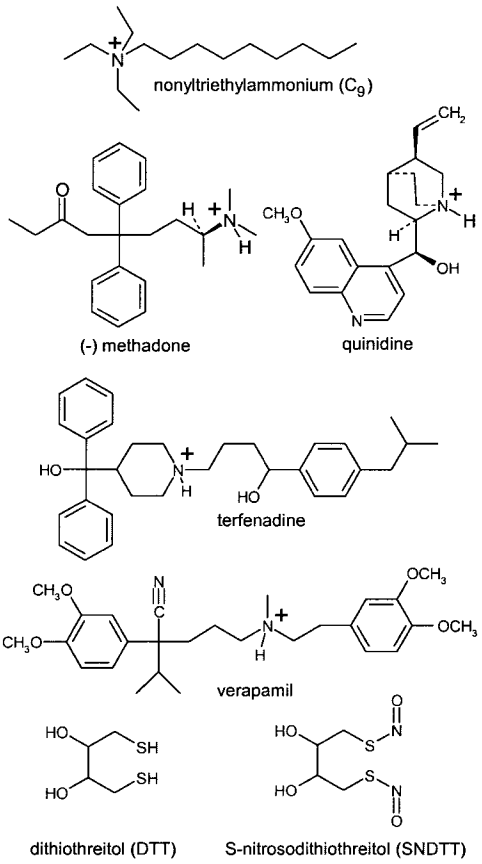

FIGURE 1. Structures of SNDTT and DTT compared with those of several QA and tertiary amine open-channel blockers. Open-channel block of squid axonal Kv channels by C_9 has been described by Armstrong (1971) and Swenson (1981). Methadone is an opioid receptor agonist that has been shown to block I_K in squid giant fiber lobe (GFL) neurons (Horrigan and Gilly, 1996). The antiarrhythmic drug quinidine produces open-channel block in the cardiac Kv1.5 channel (Snyders et al., 1992). The antihistamine terfenadine (Yang et al., 1995), and the Ca^{2+} channel blocker verapamil (Rampe et al., 1993a) also produce open-channel block in Kv1.5. All tertiary amines are shown in protonated form, which predominates at neutral pH.

nally applied tertiary amines, in contrast, can cross the membrane in their neutral form, where they reequilibrate with the active protonated form that predominates at neutral pH. In each case, apparent association rate and steady-state level of block are concentration-dependent in a manner consistent with binding of one blocker molecule per open channel. Binding affinities display a voltage sensitivity of $\sim$0.2 e_0, which is taken to reflect the sensing of roughly 20% of the membrane voltage drop by these monovalent cations in reaching their binding site. Dissociation is accelerated by high external K^+, presumably by electrostatic repulsion, suggesting that these blockers directly occlude the K^+ permeation pathway.

A more detailed architecture of the "QA cavity" has recently emerged from two main sources. First, mutational approaches with the *Shaker*B (ShB) Kv channels have shown that the residues with the greatest effect on QA affinity are located in the sixth transmembrane (S6) helix (Choi et al., 1993). Moreover, cysteine-scanning mutagenesis of ShB has demonstrated that access of cytoplasmic cysteine-modifying reagents to these S6 residues is dependent on channel opening (Liu et al., 1997), and that bound QA ions protect these residues from modification (del Camino et al., 2000). Second, the crystal structure of KcsA, a homologous bacterial channel, has revealed a sizeable cavity lined by S6 residues on the cytoplasmic side of the selectivity filter (Doyle et al., 1998).

Although the positive charge of QA ions and protonated tertiary amines probably facilitates association with a K^+ coordinating site in the channel cavity (Doyle et al., 1998; Roux and MacKinnon, 1999), hydrophobic interactions mediate the stability of the blocker–channel complex. Increasing the length of n-alkyl side chains on QA ions (Armstrong, 1969, 1971; French and Shoukimas, 1981; Swenson, 1981; Choi et al., 1993) and tertiary amines (Longobardo et al., 1998) increases affinity for the channel by decreasing the dissociation rate. Hydrophobic phenyl groups also increase affinity, but polar hydroxyl groups generally reduce affinity (Armstrong, 1971; Swenson, 1981). In a complementary manner, the hydrophobicity of channel residues also determines affinity. Substitution of more hydrophobic amino acids at certain positions in the S6 helix increases the affinity of QA ions for ShB (Choi et al., 1993), as well as the affinity of the tertiary amine quinidine for Kv1.5 (Yeola et al., 1996).

We have previously observed an accelerated inactivation of voltage-gated potassium current (I_K) in squid giant fiber lobe (GFL) neurons caused by NO donors applied in the presence of DTT (Fig. 1; Gilly et al., 1995). In this report, we demonstrate that this phenomenon is due to the direct effect of nitrosylated DTT, or S-nitrosodithiothreitol (SNDTT; Fig. 1). SNDTT induces an exponential decay of I_K through Kv1 subfamily channels that is distinct from endogenous mechanisms of channel inactivation. This effect is qualitatively similar to that caused by the more "conventional" open-channel blockers described above despite the markedly different structure of SNDTT. SNDTT has no fixed charge, and is much smaller than conventional open-channel blockers. The structure of SNDTT is also not very hydrophobic, containing only four carbons, each with a polar functional group. The unique nitrosyl groups are both required for block (i.e., one on each sulfur atom), and hydrogen bonds between these groups and the channel are a likely source of binding energy. Most significantly, results suggest that two SNDTT molecules can bind reversibly to each open channel, most likely within the channel cavity.

MATERIALS AND METHODS

Molecular Biology

A recombinant baculovirus containing the NH_2-terminal deletion mutant of *Drosophila Shaker*B cDNA (ShBΔ6–46 or ShBΔ; Hoshi et al., 1990) was a gift of Dr. Min Li (Johns Hopkins University, Baltimore, MD). Two ShBΔ mutants in the pGW1-CMV mammalian expression vector (British Biotech) were gifts of G. Yellen (Harvard University, Cambridge, MA) ShBΔ T449V, C301S, C308S ([Holmgren et al., 1996] and "Cys-less ShBΔ," in which all seven native cysteines were mutated to serine (residues 96, 301, and 308), valine (245, 286, and 505), or alanine (462; Boland et al., 1994). rKv1.1, rKv1.2, rKv1.3, rKv1.4, rKv1.5, rKv1.6, rKv2.1, rKv3.1b, and rKv4.2 were gifts of J.S. Trimmer (State University of New York-Stonybrook, Stonybrook, NY) and were all in the pRBG4 mammalian expression vector (Lee et al., 1991) except for rKv3.1b which was in the pRc/CMV expression vector (Invitrogen).

Isolation and Maintenance of GFL Neurons

Adult squid (*Loligo opalescens*) were obtained from Monterey Bay, CA and housed for up to 1 wk in circular laboratory tanks plumbed with flow-through seawater. GFL cell bodies were isolated from the posterior tip of the stellate ganglion and maintained in primary culture at 16°C as described previously (Gilly et al., 1990). Cells for I_K and I_{Ca} recordings were used for recording within 2 d of isolation. I_{Na} was recorded from a cell cultured for 13 d after isolation.

Mammalian Cell Culture

HEK 293 cells (American Type Culture Collection [ATCC]) were maintained according to standard techniques at 37°C (5% CO_2) in Dulbecco's modified Eagle medium (Life Technologies) with 10% FBS (Sigma-Aldrich), 100 U/ml penicillin, and 0.1 mg/ml streptomycin. After trypsinization, cells to be transfected were plated at ~5–10% confluency onto 5-mm-diam round coverslips (Bellco) that had been preincubated in a 1-mg/ml protamine solution. Plasmid expression constructs were introduced using $CaPO_4$ transfection. Coverslips with cells to be transfected were typically kept in 35-mm plastic petri dishes. For each dish, 0.2–3.0 μg expression plasmid in 60 μl 250 mM $CaCl_2$ was added dropwise to 60 μl of HEPES-buffered saline (HBS: 274 mM NaCl, 1.5 mM $Na_2HPO_4 \cdot 7\ H_2O$, 55 mM HEPES, pH 7.0). This mixture was immediately added dropwise to the dish, which was left undisturbed for 30–60 min at room temperature before transfer to the 37°C incubator. Cells were typically cotransfected with a green fluorescent protein (GFP) expression construct (pEGFP-N1; CLONTECH). This allowed cells expressing recombinant protein to be identified by fluorescence microscopy (IMT-2 microscope with BH2-RFC fluorescence attachment; Olympus), with no discernible effect on functional channel properties or SNDTT action.

Maintenance and Infection of Sf9 Cells

Spodoptera frugiperda cells of the Sf9 line (ATCC) were maintained in suspension at 27°C in Grace's insect medium (Life Technologies) supplemented with 3.3 mg/ml lactalbumin hydrolysate, 3.3 mg/ml yeastolate, 50 μg/ml streptomycin, 50 U/ml penicillin, 1.25 μg/ml fungizone, and 10% FBS (Sigma-Aldrich) according to standard protocols (Summers and Smith, 1987). For infections, log-phase cells were seeded in 35-mm culture dishes at 10^6 cells/ml and allowed to attach for 30–60 min. The media was then removed and inoculum was added at a multiplicity of infection of 5–10. After 1 h, the inoculum was replaced with fresh medium.

Electrophysiology

Recordings from HEK 293 and Sf9 cells were obtained with an EPC7 amplifier (HEKA) using standard whole-cell patch-clamp techniques. Recordings from GFL cells were obtained using an amplifier of conventional design with a 20-MΩ feedback resistor. Cell and pipet capacitance transients were cancelled using the amplifiers. Linear leak and residual capacity currents were subtracted using a P/−4 protocol at a holding potential of either −80 or −100 mV. Series resistance was compensated electronically as much as possible, typically to an effective final value of ~1 MΩ. Data sampling and pulse generation were controlled with software written by Dr. D.R. Matteson (University of Maryland, Baltimore, MD). Electrodes of 0.5–1.5 MΩ resistance were pulled from borosilicate glass (for HEK 293 and Sf9 cells; VWR) or 7052 glass (for GFL cells; Garner), fire polished, and coated with Sylgard (Dow Corning) to reduce pipet capacitance. Holding potential was −80 mV throughout. Current output was filtered at 5.0–10.0 kHz for sampling at 20 kHz and down to 1 kHz for 2-kHz sampling. GFL recordings were made at 18°C. Recordings from HEK 293 and Sf9 cells were made at ambient temperature (19–22°C)

Physiological solutions for GFL cells were as follows (in mM except where noted): for I_K internal, 20 KCl, 80 potassium glutamate, 50 KF, 5 lysine, 1 EGTA, 1 EDTA, 381 glycine, 291 sucrose, and 10 HEPES, pH 7.8; for I_K external, 10 KCl, 470 NaCl, 10 $CaCl_2$, 20 $MgCl_2$, 20 $MgSO_4$, 200 nM TTX, and 10 HEPES, pH 7.8; for I_{Na} internal, 100 sodium glutamate, 50 NaF, 50 NaCl, 10 Na_2EGTA, 300 tetramethylammonium (TMA) glutamate, 25 TEA-Cl, and 10 HEPES, pH 7.8; for I_{Na} external, 480 NaCl, 10 $CaCl_2$, 20 $MgCl_2$, 20 $MgSO_4$, and 10 HEPES, pH 7.8; for I_{Ca} internal, 20 TMA-Cl, 80 TMA-glutamate, 50 TMA-F, 5 lysine, 381 glycine, 291 sucrose, 1 EGTA, 1 EDTA, and 10 HEPES, pH 7.9; and for I_{Ca} external, 60 $CaCl_2$, 480 TMA-Cl, 10 TEA-Cl, 200 nM TTX, and 10 HEPES, pH 7.7.

Physiological solutions for HEK 293 cells were as follows (in mM): for internal, 90 KCl, 60 KF, 2 $MgCl_2$, 10 EGTA, 10 HEPES, 80 sucrose, and 25 KOH, pH 7.0; for external, 20 KCl, 180 NaCl, 4 $CaCl_2$, 5 $MgCl_2$, 10 HEPES, and 0.1 EDTA, pH 7.2.

Physiological solutions for Sf9 cells were as follows (in mM): for internal, 20 KCl, 50 KF, 80 potassium glutamate, 26 glycine, 5 lysine, 85 sucrose, 1 EGTA, 1 EDTA, 10 HEPES, and 4 TMA-OH, pH 7.0; and for external, 20 KCl, 120 NaCl, 10 $CaCl_2$, 10 $MgCl_2$, 10 $MgSO_4$, and 5 HEPES, pH 7.2.

External solution was changed with a flow-through system.

Series Resistance Errors

Although voltage errors due to residual (uncompensated) series resistance were typically small in this study (<10 mV), it is important to consider what kind of systematic artifacts these errors could introduce. Two particular sets of data (voltage dependence of steady-state block, and dose–response experiments) may be particularly susceptible to contamination.

Possible contributions of series resistance to the observed voltage dependence of SNDTT binding were investigated in the following manner. First, the corrected voltage (V_{SNDTT}) for each measurement in the presence of SNDTT was calculated as $V_{SNDTT} = V_{com} - I_{SNDTT}R_S$, where V_{com} is the command voltage, I_{SNDTT} is steady-state I_K in SNDTT, and R_S is the effective series resistance. Second, voltages ($V_{control}$) for control I_K ($I_{control}$) were corrected in the same manner, and a corrected $I_{control} - V_{control}$ relationship was plotted. This relationship was linear above 0 mV for all cells, and the proper $I_{control}$ at V_{SNDTT} was determined by extrapolation. Corrected values for the ratio of blocked to open channels (B/O) could then be calculated and plotted as in Fig. 5 C. This correction procedure did not detectably alter the apparent valence of approximately $-0.3\ e_0$.

An elaboration on this procedure was used to examine possible effects of series resistance on the shape of the dose–response relationship for SNDTT. Series resistance would preferentially affect determination of the fractional block, f_B, at high SNDTT concentrations, where differences between $V_{control}$ and V_{SNDTT} would be maximal. This trend might generate an artificially complex dose–response relationship, and the voltage dependence of steady-state block could further complicate the situation. A cell with relatively high voltage error (~13 mV at V_{com} = +40 mV for $I_{control}$) was analyzed in the following manner. Extrapolation of $I_{control}$ was performed as above to provide estimates of corrected B/O at V_{SNDTT} for each SNDTT concentration. The observed exponential voltage dependence of B/O (−0.3 e_0; see Fig. 5 C) was then used to calculate the corrected B/O value of each concentration at +40 mV. Dose–response curves (f_B versus SNDTT concentration) constructed from these data were virtually indistinguishable from uncorrected data.

Nitrosothiol Synthesis

For each application, racemic (D, L) SNDTT was synthesized by mixing equal volumes of the following stock solutions, which were prepared in the extracellular recording solutions described above: 100 mM D,L-DTT, 300 mM HCl; and 200–300 mM $NaNO_2$. At low pH, NO_2 is a NO+ donor, and readily nitrosylates thiol groups (Arnelle and Stamler, 1995). Reaction of thiol with equimolar NO_2 under these conditions is reportedly complete, with virtually no remaining NO_2 (Arnelle and Stamler, 1995). The two- to threefold excess of NO_2 over DTT ensures that both thiol groups on the DTT molecule are nitrosylated (Le et al., 1997), and this reactant ratio was used throughout, except in specific experiments that are indicated. The resulting 50-mM SNDTT solution was diluted in physiological solutions, and the pH was adjusted using NaOH. The nitrosylated monothiols S-nitroso-β-mercaptoethanol and S-nitroso-l-thioglycerol were prepared from β-mercaptoethanol and l-thioglycerol respectively, using the synthesis described above, but with a 1:1 NO_2/thiol ratio. All reagents were purchased from Sigma-Aldrich.

Accounting for SNDTT Breakdown

The instability of SNDTT in solution has been described previously (Arnelle and Stamler, 1995; Le et al., 1997). Consistent with the intramolecular nature of the underlying breakdown reaction, the time dependence of SNDTT concentration was well described by a single exponential decay (see Fig. 7). Relative differences in applied SNDTT concentrations should therefore be preserved at matched times after synthesis. This prediction was verified in experiments where the time course of SNDTT concentration (assayed by absorbance at 333 nm) was monitored after the synthesis of different starting concentrations (not shown). Absorbance was measured with a spectrophotometer (model BioSpec-1601; Shimadzu). Except where specified, comparisons of SNDTT blocking properties were obtained at ~4 min, at which point, ~25% of synthesized SNDTT has broken down. SNDTT concentrations have not been corrected, and consequently, f_B and B/O values are slight underestimates for a stated SNDTT concentration. The shape of dose–response curves should be unaffected, but best-fit values for dissociation constants are overestimates by ~25%. The time course of recovery from SNDTT block was found to be largely independent of concentration (not illustrated), and two-pulse recovery protocols could thus be performed at various times after synthesis.

To avoid directional bias due to SNDTT breakdown, the sequence of voltage amplitudes for I_K families (see Fig. 5) was randomized, as was the order of recovery intervals in two-pulse protocols (see Figs. 3 and 10).

Data Analysis and Presentation

Fitting routines and visual preparation of data were performed with the Igor Pro software package (Wavemetrics). Estimated standard errors of fitting parameters were calculated using Prism (GraphPad).

RESULTS

Block of I_K in Squid Giant Fiber Lobe Neurons by SNDTT

Time-dependent block of Kv channels by SNDTT was first observed in squid GFL neurons as a DTT-dependent acceleration of I_K inactivation by NO donor compounds (Gilly et al., 1995). Whole-cell recordings from GFL neuronal cell bodies are shown in Fig. 2. At positive membrane voltages, I_K inactivates slowly to ~65% completion with a time constant (τ) of ~75 ms. Neither DTT nor the NO donor S-nitroso-*N*-acetylpenicillamine (SNAP) have a marked effect on I_K when applied alone at 5-mM concentrations (Fig. 2 A). When applied in combination, however, 5 mM SNAP and 5 mM DTT induce a rapid exponential relaxation of I_K ($\tau \approx 15$ ms) resulting in a 70% reduction in steady-state I_K at the end of the pulse (Fig. 2 B). Early activation kinetics are not affected, however. The effect of SNDTT reverses immediately upon solution washout. Qualitatively similar results are produced by other NO donors (S-nitrosocysteine, S-nitrosoglutathione, and diethylamine-NO) only when combined with DTT (not illustrated). Reducing agents other that DTT (glutathione, β-mercaptoethanol), however, are ineffective when combined with these NO donors (not illustrated). Pretreatment of channels with DTT, followed by the application of an NO donor in the absence of DTT, is also ineffective (not illustrated).

This pattern of results suggests that a nitrosylation reaction specifically involving DTT is critical for the effect. A nitrosyl group such as that on SNAP can be directly transferred to a free thiol group in a reaction known as transnitrosation. To address the possibility that nitrosylation of DTT itself underlies the SNAP-DTT effect, the two thiol groups of DTT were directly nitrosylated without an organic NO donor compound by reaction with NO_2 at low pH (Arnelle and Stamler, 1995). A twofold excess of NO_2 is sufficient to nitrosylate both thiols on DTT (Le et al., 1997), and for the purpose of the current study, SNDTT will refer exclusively to this doubly nitrosylated form.

Results in Fig. 2 C demonstrate that the application of 1 mM SNDTT is sufficient to induce a rapid exponential decay of I_K and a reduction in steady-state I_K amplitude, which are effects virtually identical to those of 5 mM SNAP + 5 mM DTT. These effects also reverse upon washout. GFL neurons also display voltage-gated Na^+ (I_{Na}) and Ca^{2+} (I_{Ca}) currents, neither of which is altered by 1 mM SNDTT (Fig. 2 D), suggesting that SNDTT is selective for K^+ channels among the voltage-gated ion channel superfamily.

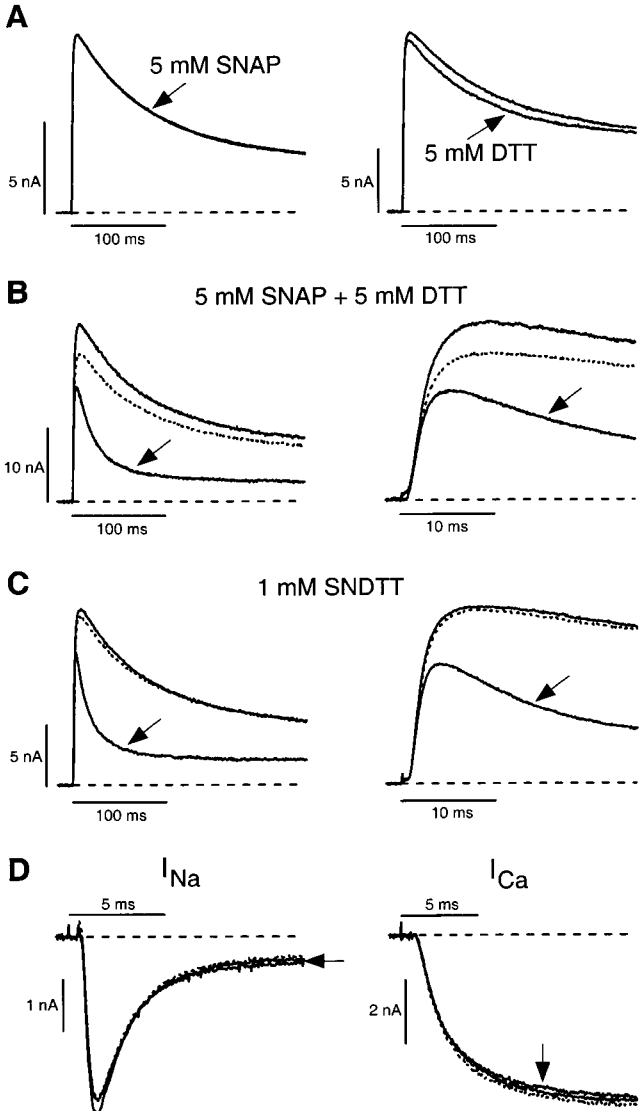

FIGURE 2. Block of squid GFL Kv channels by SNDTT. Whole-cell currents from GFL cells were evoked with depolarizations from a holding potential of −80 mV to positive voltages. The onset of the depolarization for each panel coincides with the left end of the horizontal scale bar. All solutions were bath-applied. (A) Neither 5 mM SNAP (left) nor 5 mM DTT (right) significantly alter I_K at +60 mV. In both panels, control I_K is unmarked, and I_K in the presence of compound is indicated with an arrow. Control and SNAP traces superimpose in the left panel. (B) Effect of simultaneously applied 5 mM SNAP + 5 mM DTT on I_K during long (250 ms; left) and short (25 ms; right) depolarizations to +60 mV. Pre-application control I_K is unmarked, I_K in the presence of SNAP + DTT is indicated with an arrow, and I_K after washout is dotted. (C) Effect of 1 mM SNDTT on I_K during long and short depolarizations to +30 mV. Markings are as in B. (D) 1 mM SNDTT has no effect on I_{Na} (left) or I_{Ca} (right). Solutions are described in MATERIALS AND METHODS. I_{Na} and I_{Ca} were evoked with depolarizing steps to +10 and 0 mV, respectively. Markings are as in B.

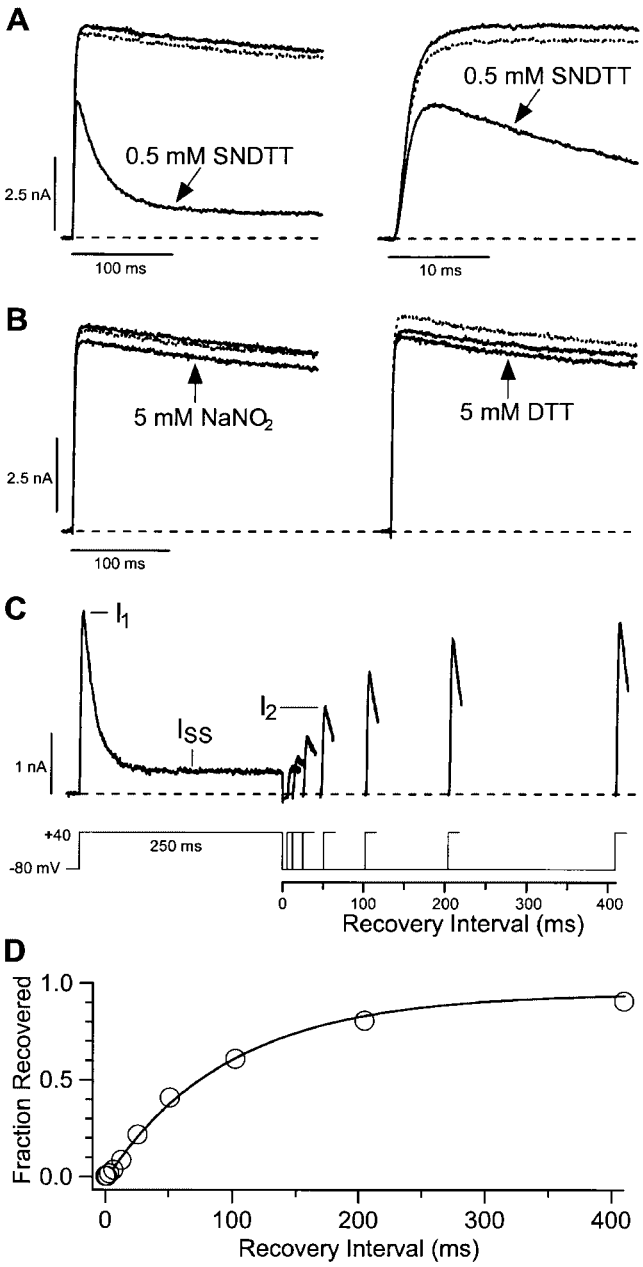

FIGURE 3. Block of *Shaker* K^+ channels by SNDTT. Whole-cell I_K in HEK 293 cells expressing ShBΔ channels (ShBΔ I_K) was evoked with depolarizations to +40 mV. (A) I_K is illustrated for pulses of 250 ms (left) and 25 ms (right) before bath application of SNDTT (unmarked), in the presence of 0.5 mM SNDTT (arrow), and after washout (dotted). Onset times of the depolarizations coincide with the left end of the horizontal scale bars. (B) Reactants used to synthesize SNDTT are ineffective. $NaNO_2$ (left) and DTT (right) were individually applied at 5-mM concentration to the same cell with an intervening washout. Sensitivity of I_K in this cell to SNDTT was verified (not illustrated). Markings are as in A. (C) Recovery of ShBΔ at −80 mV from block by 0.5 mM SNDTT is demonstrated using the illustrated two-pulse protocol. (D) Time course of recovery from SNDTT block. The fraction of channels that were blocked by SNDTT during the first depolarization and have recovered by the time of the second depolarization (*Fraction Recovered*) is calculated as: $\textit{Fraction Recovered} = (I_2 - I_{SS})/(I_1 - I_{SS})$, where I_1 and I_2 represent peak I_K during the first and second pulse respectively, and I_{SS} represents the steady-state I_K of the first pulse. The solid line is a single exponential fit with a time constant of 97 ms.

Basics of Shaker Channel Block by SNDTT

SNDTT is also a potent blocker of the ShB Kv1 channel (Fig. 3). In whole-cell recordings of HEK 293 cells expressing the N-type inactivation-removed ShBΔ6–46 channel (ShBΔ; Hoshi et al., 1990), bath-applied SNDTT causes a characteristic exponential decrease in I_K after a normal early activation time course (Fig. 3 A). The reactants for SNDTT synthesis ($NaNO_2$ and DTT) have virtually no effect (Fig. 3 B). This channel was chosen for further characterization of SNDTT block because of its high affinity for SNDTT (see Fig. 4), the availability of noninactivating mutants, and a large body of existing structure–function data (for review see Yellen, 1998).

Most experiments in the present study, including those illustrated in Fig. 3, used ShBΔ with three additional mutations: T449V, C301S, and C308S. The T449V mutation greatly reduces the extent of C-type inactivation (Lopez-Barneo et al., 1993), which might partially obscure a simultaneous time-dependent process such as open-channel block. Replacement of cysteines 301 and 308 with serine eliminates the current-reducing effect of intracellular cysteine-modifying reagents on wild-type ShBΔ (Holmgren et al., 1996) and prevents possible side effects due to nitrosylation of these sensitive cysteines by SNDTT or NO. In comparisons with wild-type ShBΔ in HEK 293 cells, these mutations had no discernible effect on the SNDTT blocking properties described in this report (results not shown). Therefore, for simplicity, we refer to the mutant described above as ShBΔ.

Recovery from block by SNDTT occurs at hyperpolarized voltages where channel closing is favored. Results of a standard two-pulse protocol are shown in Fig. 3 C for recovery at −80 mV. Channels blocked during the first pulse (I_1-I_{SS}) gradually recover and become available to contribute to the I_K peak for a second pulse (I_2-I_{SS}), and recovery proceeds with a time constant of ~100 ms (Fig. 3 D). More detailed studies of recovery phenomena, including effects of voltage and external K^+, will be examined in a forthcoming report.

Binding Affinity and Stoichiometry

Block of open channels has routinely been interpreted in the literature using the following scheme:

$$N \text{ x blocker (S)} + \text{open channel (O)} \overset{K_d}{\longleftrightarrow} \text{blocked channel (B)}$$

(SCHEME I)

where N represents the number of molecules of blocker S necessary to occlude the channel, and K_d represents the dissociation constant for the reaction. The steady-state fraction of channels blocked (f_B) is used throughout this report as a measure of blocker efficacy. For Scheme I, f_B is related to the concentration of blocker [S] and dissociation constant K_d by the equation:

$$f_B = \left(1 + \frac{K_d}{[S]^N}\right)^{-1}. \quad (1)$$

Dose–response data for conventional open-channel blockers are well described by Eq. 1 with $N = 1$, which is consistent with a blocker-channel stoichiometry of 1:1.

Results from an experiment in which a range of SNDTT concentrations was applied to a single 293 cell expressing ShBΔ is illustrated in Fig. 4 A. Increasing SNDTT concentrations cause a faster decay of I_K and a decreased steady-state I_K, which are effects that qualitatively resemble those of conventional open-channel blockers. The decay of I_K at lower SNDTT concentrations (≤0.1 mM) is obviously contaminated by the slow endogenous inactivation seen in the control I_K trace. Therefore, it is unclear in these traces whether block has proceeded to the steady-state levels necessary for an accurate determination of the dose–response relationship for SNDTT. Inactivation could be effectively factored-out, however, by performing a point-wise division of each I_K trace in the presence of SNDTT by its respective control I_K trace. Assuming inactivation and block proceed independently, this transformation provides a running measure of the fraction of channels not blocked ($1 - f_B$). In these normalized traces, block appears to reach a virtual steady-state by 740 ms for all concentrations (Fig. 4 B).

The relationship between steady-state f_B and SNDTT concentration is illustrated in Fig. 4 C, where mean $f_B \pm$ SEM is plotted for four cells that were each subjected to every concentration plotted. Fits of Eq. 1 with either $N = 1$ or 2 are quite poor (Fig. 4 C). With $N = 1$ (Fig. 4 C, dotted curve), the curve is generally too shallow, whereas for $N = 2$ (Fig. 4 C, dashed curve) it is too steep. Although a reasonable fit can be obtained for $N = 1.4$ (Fig. 4 C, solid curve), the physical meaning of this is obscure. Arbitrary shifting of the $N = 1$ and 2 curves provides insight into the apparent intermediate nature of the data: $N = 1$ provides a close fit to the data at low concentrations ($<10^{-4}$ M), whereas $N = 2$ yields a close fit for higher concentrations ($>10^{-4}$ M). This observation suggests that the binding mechanism of SNDTT is more complex than that described by Scheme I and Eq. 1, the strict interpretation of which requires that binding of N blockers occur simultaneously.

In light of the unclear physical interpretation of Scheme I with $N = 1.4$, and with no a priori reason to believe that binding of more than one SNDTT molecule should be simultaneous, Scheme I and Eq. 1 are of limited mechanistic applicability. Therefore, we considered less constraining schemes in which two molecules can bind sequentially.

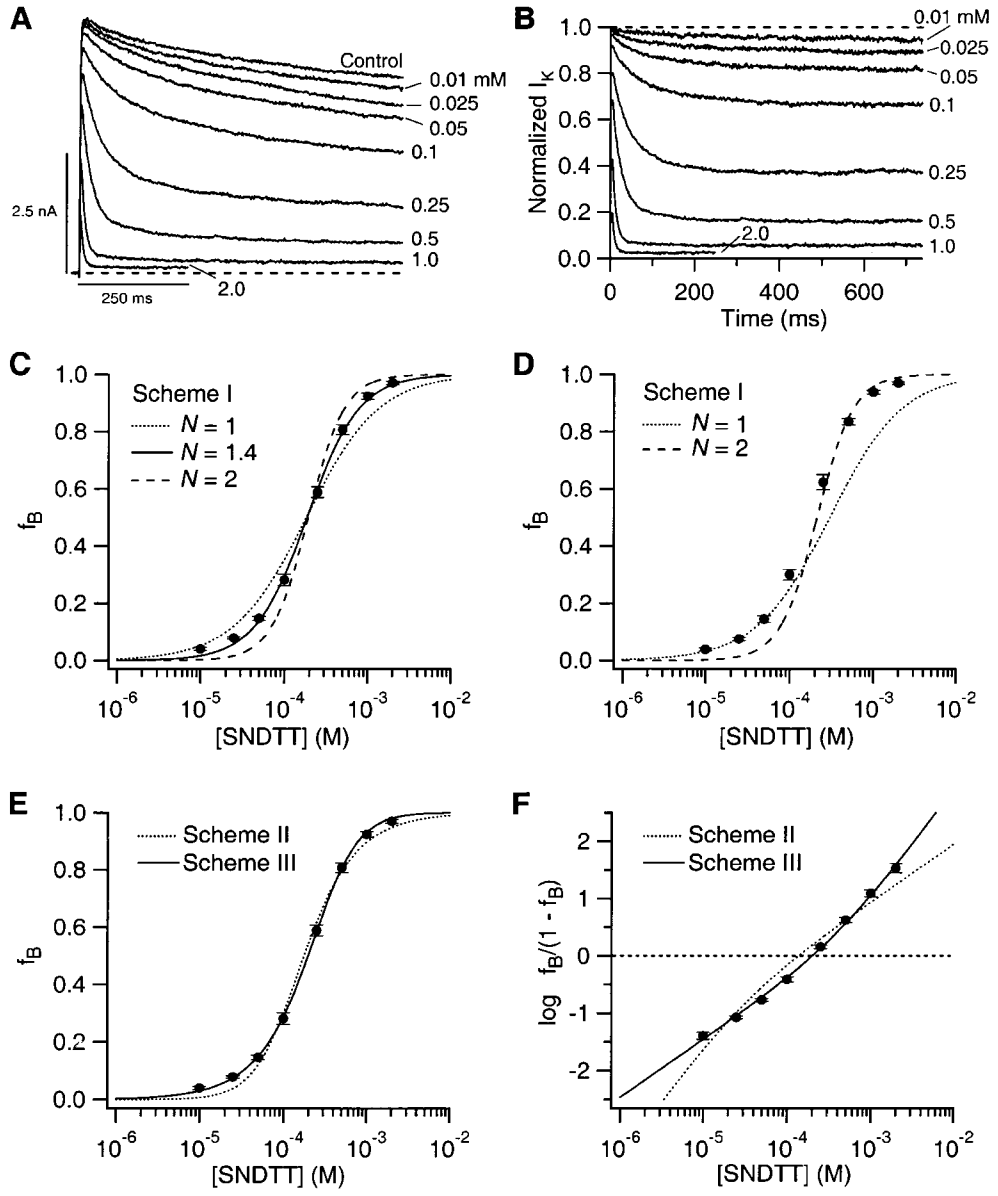

FIGURE 4. Concentration dependence of SNDTT block. (A) ShBΔ I_K at +40 mV in the presence of the indicated concentrations of SNDTT is compared with a pre-application control. The application of each concentration was followed by a wash with normal external solution. To account for variation (~10%) in control I_K amplitude over the course of the experiment, I_K traces in the presence of SNDTT were scaled by factors necessary to standardize the amplitudes of respective pre-application controls. (B) Traces for I_K in the presence of SNDTT from A were normalized by performing a point-wise division by the respective preapplication control traces. (C–E) Dose–response plots for SNDTT. The steady-state fraction of channels blocked (f_B) at +40 mV was calculated as $1 - (I_{SNDTT}/I_{control})$, where $I_{control}$ and I_{SNDTT} represent I_K in the absence and presence of SNDTT, respectively. Data represent means ± SEM for four cells. (C) Least-squares fits of a standard binding curve with integer values of N (Scheme I, Eq. 1 from RESULTS) either underestimate ($N = 1$; $K_d = 0.18 \pm 0.02$ mM; dotted curve) or overestimate ($N = 2$; $K_d = 3.7 \times 10^{-8} \pm 0.7 \times 10^{-8}$ M^2; dashed curve) the slope of the data. The solid line represents a fit of Scheme I for which N remained a free parameter, with best fit values of $N = 1.4 \pm 0.1$ and $K_d = 6.6 \times 10^{-6} \pm 2.8 \times 10^{-6}$ M$^{1.4}$. (D) Scheme I: $N = 1$ (dotted) and $N = 2$ (dashed) curves can be arbitrarily positioned to fit data at low (0.01–0.05 mM) and high (0.25–2.0 mM) concentrations respectively. K_d values for the illustrated curves are 0.3 mM ($N = 1$) and 4.5×10^{-8} M^2 ($N = 2$). (E) A scheme in which two molecules can bind to the channel sequentially, but only one is required for block (Scheme III, Eq. 3 from RESULTS; solid curve) provides the best fit to the data. Best fit dissociation constants for the binding of the first (K_{d1}) and second molecules (K_{d2}), were 0.67 ± 0.03 mM and 0.14 ± 0.02 mM, respectively. A sequential model in which binding of both molecules is required for block (Scheme II, Eq. 2 from Results; dotted curve) underestimates the data at low and high concentrations. Best-fit values for dissociation constants were $K_{d1} = 0.25 \pm 0.04$ mM and $K_{d2} = 0.051 \pm 0.004$ mM. The chi-squared value for Scheme III is ~20-fold lower than that of Scheme II. (F) Hill plots with fits of Schemes II and III. Y values were transformed as indicated in the axis label. Least-squares fits of the Hill equation for Scheme III (solid curve):

$$\log(f_B/(1 - f_B)) = \log\left(\frac{[S]}{\frac{1}{2}K_{d1}} + \frac{[S]^2}{K_{d1}K_{d2}}\right)$$

yielded values for dissociation constants of $K_{d1} = 0.58 \pm 0.04$ mM and $K_{d2} = 0.21 \pm 0.03$ mM. Best fit values for the Scheme II Hill equation (dotted curve):

$$\log(f_B/(1 - f_B)) = \log\left(\frac{2K_{d2}}{[S]} + \frac{K_{d1}K_{d2}}{[S]^2}\right)^{-1}, \quad (1)$$

were $K_{d1} = 0.058 \pm 0.043$ mM and $K_{d2} = 0.056 \pm 0.015$ mM.

A sequential mechanism in which the binding of both molecules is required for block can be schematized as:

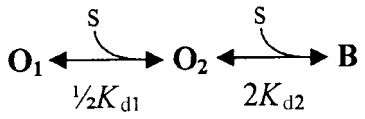

(SCHEME II)

$$f_B = \frac{B}{O_1 + O_2 + B} = \left(1 + \frac{2K_{d2}}{[S]} + \frac{K_{d1}K_{d2}}{[S]^2}\right)^{-1}, \quad (2)$$

where $\mathbf{O_1}$ represents an unliganded conducting state of the channel, $\mathbf{O_2}$ represents a conducting state with one blocker molecule bound, and **B** represents a blocked state with two blocker molecules bound. Alternatively, binding at either one of the two sites may be sufficient to occlude the channel, and the corresponding scheme is:

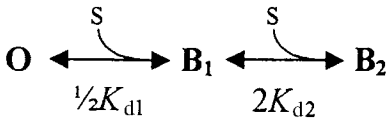

(SCHEME III)

$$f_B = \frac{B_1 + B_2}{O + B_1 + B_2} = \left(1 + \frac{1}{\frac{[S]}{\frac{1}{2}K_{d1}} + \frac{[S]^2}{K_{d1}K_{d2}}}\right)^{-1}, \quad (3)$$

where **O** represents an unliganded conducting state, $\mathbf{B_1}$ represents a blocked channel with one blocker molecule bound, and $\mathbf{B_2}$ represents a blocked channel with a second blocker bound. K_{d1} and K_{d2} in both cases represent the dissociation constants for the binding of the first and second blocker molecules respectively. The coefficients preceding K_{d1} and K_{d2} are derived in APPENDIX, and are related to the assumption that binding of the first blocker (K_{d1}) can occur at either of two intrinsically identical sites in the channel, whereas binding of the second blocker (K_{d2}) must take place at the remaining site. Cooperativity will be reflected in a value for K_{d2} that differs from that of K_{d1}. Eqs. 2 and 3 give the relationships between f_B and K_{d1} and K_{d2}, with symbols for states representing the respective steady-state probabilities.

Fits of Scheme II and III to the data are illustrated in Fig. 4 E. Scheme II fits the data satisfactorily only around $f_B \approx 0.5$, and significantly underestimates the data at both low and high concentrations. Scheme III, however, provides a very good fit over the entire concentration range, with well-constrained values (± standard errors) for the binding of the first and second SNDTT molecules of $K_{d1} = 0.67 \pm 0.03$ mM and $K_{d2} = 0.14 \pm 0.02$ mM, respectively. The reduced slope at low concentrations and steeper slope at higher concentrations is a fundamental property of Eq. 3. At low concentrations ($<2K_{d2}$) Scheme III is approximated by a Scheme I: $N = 1$ curve, and at higher concentrations, approaches an Scheme I: $N = 2$ curve (see APPENDIX). The opposite relationship is true of Scheme II. This qualitative distinction is emphasized in a Hill plot with fits for Schemes II and III (Fig. 4 F). The aforementioned $N = 1$ and $N = 2$ regions are linearized into segments with slope = N, and again the data are in much better qualitative (regarding directionality of the curve) and quantitative (regarding closeness of the fit) agreement with the fit of Scheme III.

Analysis of dose–response curves for the four individual cells gave results similar to the mean data, arguing that the shape of the mean curve is not an artifact of averaging. Fits to individual cells (not illustrated) produced minimized chi-squared values for Scheme III that were 6–15-fold less than those for Scheme II, and 20–100-fold less than those for Scheme I ($N = 1$ or 2). The best-fit values for K_{d1} and K_{d2} showed low variability from cell to cell ($K_{d1} = 0.69 \pm 0.06$ mM, $K_{d2} = 0.14 \pm 0.02$ mM; mean ± SEM for four cells). Again, only Scheme III generated fits from which the data did not systematically deviate.

Voltage Dependence of Block

Conventional open-channel blockers universally show increased block at more positive voltages, consistent with a binding site for these cationic compounds that lies within the membrane voltage field. For these Scheme I: $N = 1$–type blockers, it is convenient to examine the ratio of blocked to open channels (B/O), which displays an exponential voltage dependence reflecting that of the dissociation constant:

$$B/O = \frac{[S]}{K_d(0)e^{-qVF/RT}} = B/O(0)e^{qVF/RT}.$$

In this equation, $K_d(0)$ and $B/O(0)$ represent values at 0 mV, q represents equivalent charge movement, V is voltage, and F, R, and T have standard meanings (see Fig. 5 legend for definitions). Although the voltage dependence of B/O will obviously be more complex for Scheme III, interpretation is simplified at higher concentrations ($>2K_{d2} \approx 0.28$ mM; see APPENDIX), where:

$$B/O \approx \frac{[S]^2}{K_{d1}K_{d2}}.$$

The voltage dependence of B/O at high concentrations,

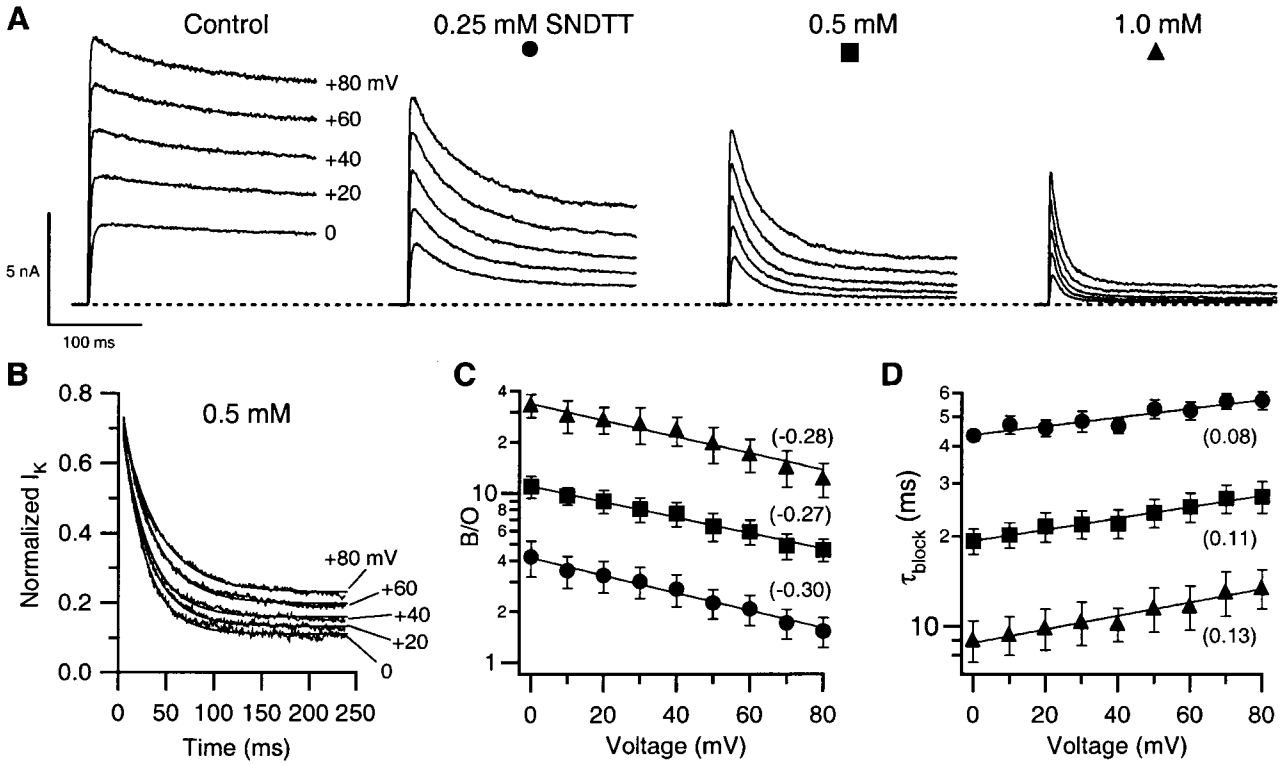

FIGURE 5. Voltage dependence of SNDTT block. (A) ShBΔ I_K records are illustrated at the indicated voltages in the presence of the indicated concentrations of SNDTT. All records are from a single cell. The application of each concentration was preceded by the acquisition of control records in normal external solution, and control I_K at a given voltage varied by <10% over the course of the experiment. Symbols associated with concentrations are used in C and D. (B) The I_K family for 0.5 mM SNDTT was normalized to controls as described for Fig. 4 B. Single exponential fits are superimposed. (C) The ratio of blocked to open channels (B/O) at the end of a 250-ms depolarization was calculated at voltages between 0 and +80 mV using the equation, $B/O = (I_{control} - I_{SNDTT})/I_{SNDTT}$, where $I_{control}$ and I_{SNDTT} represent I_K in the absence and presence of SNDTT, respectively. (C) τ_{block} was derived from least-squares fits of single exponentials to normalized I_K traces at voltages between 0 and +80 mV, as shown in B. Symbols (corresponding to SNDTT concentrations in A) and associated error bars represent means ± SEM for six cells. Numbers in parentheses in C and D represent equivalent charge movement q for least-squares fits (solid lines) to the generic equation: $A = A(0)\ e^{qVF/RT}$, where A represents y-axis amplitude, $A(0)$ represents amplitude at 0 mV, F is Faraday's constant, R is the universal gas constant, and T is absolute temperature (293°K).

$$B/O \approx \frac{[SNDTT]^2}{K_{d1}(0)e^{-q_1 VF/RT} K_d(0)e^{-q_2 VF/RT}}$$
$$= B/O(0)e^{q_t VF/RT},$$

will reflect the sum, q_t, of the equivalent charge movements for the first (q_1) and second (q_2) binding events.

Surprisingly, the steady-state level of block by SNDTT is voltage-dependent, despite the electrical neutrality of this compound (Fig. 5). Block weakens at more positive voltages, however, an effect opposite to that for conventional open-channel blockers. The voltage dependence of B/O for SNDTT was examined at voltages where g_K for ShBΔ is maximal (>0 mV) to allow analysis of voltage-dependent binding properties independently of channel activation gating. I_K families in the presence of several relatively high concentrations of SNDTT are shown in Fig. 5 A along with a control family in the absence of SNDTT. Reduced block at more positive voltages can be qualitatively recognized by the greater spacing between I_K traces at more positive voltages. Fig. 5 B shows the I_K family for 0.5 mM SNDTT, after normalization to control I_K as described for Fig. 4 B. In this case, relief of block is evidenced by the increasing steady-state amplitudes of normalized I_K at more positive voltages.

This trend is confirmed in plots of B/O versus voltage (Fig. 5 C), where data represent means ± SEM for four cells. At each SNDTT concentration, B/O varies exponentially with voltage, with an equivalent charge movement q_t of approximately $-0.3\ e_0$, roughly equal in magnitude (but opposite in sign) to that observed with conventional open-channel blockers. For cationic blockers such as QA ions or protonated tertiary amines, such equivalent charge movement is typically expressed as zδ, where z represents the valence of the blocker, and δ is interpreted as the fraction of the membrane voltage field sensed by the blocker in reaching its binding site (Woodhull, 1973). Because SNDTT has no fixed charge, the interpretation of this voltage dependence is less straightforward. Alternative sources for

this voltage dependence are presented in DISCUSSION. As described in MATERIALS AND METHODS, correction for errors arising from uncompensated series resistance had negligible effects on this voltage dependence.

Macroscopic kinetics of block are also moderately voltage-dependent (Fig. 5 D). After normalization to factor out inactivation, the decay of I_K in the presence of SNDTT was generally well described by a single exponential, and representative fits are superimposed on the normalized I_K family shown in Fig. 5 B. Time constants (τ_{block}) derived from such fits are plotted versus voltage in Fig. 5 D as means ± SEM for six cells. At each concentration, block was slowed by more positive voltages, with an equivalent charge movement of ~0.1 e_0. While arguably shallow, this voltage dependence is significant. At each concentration, τ_{block} at +80 mV was significantly higher than at 0 mV ($P < 0.05$ by t test).

SNDTT Breakdown

SNDTT is known to break down spontaneously in solution via an intramolecular reaction resulting in the formation of "oxidized DTT" (trans-4,5-dihydroxy-1,2-dithiane) and the simultaneous liberation of two NO radicals (Fig. 6 A; Arnelle and Stamler, 1995; Le et al., 1997). Data illustrated in Fig. 6 B demonstrate that these breakdown products have negligible effects on ShBΔ I_K. Although NO can undergo further reactions with O_2 in solution (for review see Stamler et al., 1992), the ineffectiveness of the NO donor SNAP argues that the products of such reactions are not active. Although our data (see below) and those of others (Le et al., 1997) argue for "doubly- nitrosylated" DTT as the overwhelming product when the NO_2/DTT synthesis ratio is ≥2, the unique breakdown products of "singly-nitrosylated" DTT (Arnelle and Stamler, 1995) were also tested for effect, using rat Kv1.1 channels. None of these compounds (NH_2OH, N_2O, and NO^-) reproduced to any extent the effect of SNDTT (data not illustrated; see Fig. 11 for effects of SNDTT on Kv1.1).

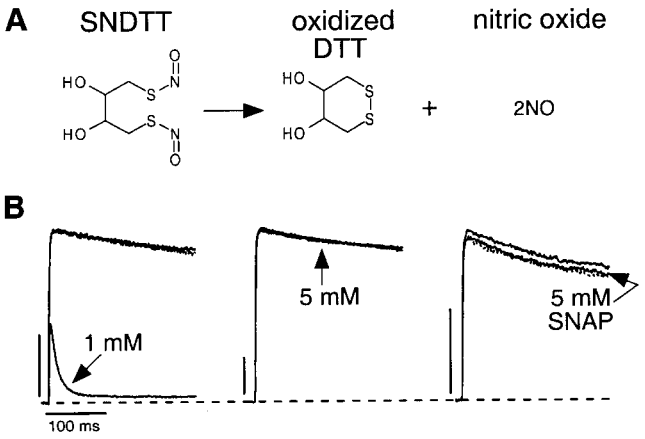

FIGURE 6. Breakdown products of SNDTT do not cause block. (A) Reaction for spontaneous breakdown of SNDTT (see RESULTS). (B) The effect of bath-application of each compound in A on ShBΔ I_K at +40 mV is illustrated below the corresponding structure. For each compound, I_K is shown before application (unmarked), in the presence of the compound (arrow), and after washout (dotted). The effect of NO was assayed using the NO donor SNAP. The resulting concentration of NO in solution was not measured, however. Compounds were tested on individual cells. Scale bars are all 2.5 nA.

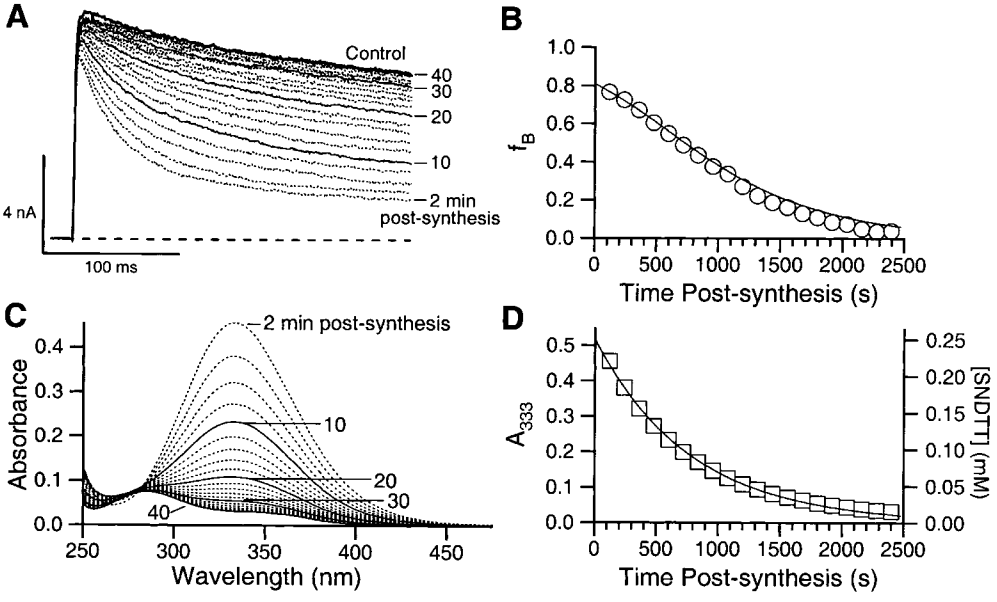

FIGURE 7. Spontaneous breakdown of SNDTT. (A) Time-dependent disappearance of the blocking effect of SNDTT on ShBΔ I_K. After the application of 0.25 mM SNDTT, I_K traces at +40 mV were acquired at 2-min intervals beginning two minutes post-synthesis. The top trace is a pre-application control. (B) Time course of the decrease in fraction of channels blocked (f_B) at the end of the records displayed in A. The smooth curve is the prediction of Scheme III as described in RESULTS. (C) Disappearance of the SNDTT absorbance spectrum over time. Spectra for SNDTT prepared in a manner identical to that for panel A were acquired at the same time points as in A. (D) Breakdown of 0.25 mM SNDTT over time after synthesis. The relative SNDTT concentration was monitored using the absorbance at 333 nm (A_{333}). The smooth curve is a least-squares exponential fit with a time constant of 773 ms with a time-zero amplitude of 0.52. The right-hand axis gives SNDTT concentration based on 0.25 mM at time zero.

SNDTT breakdown is evident in a slow diminution of the SNDTT effect over the course of an experiment. After application of SNDTT, the steady-state level and rate of block decrease in parallel over time, such that I_K eventually returns to match preapplication controls (Fig. 7 A). This effect is more pronounced at the higher temperature used for ShBΔ-HEK 293 cell experiments (21 vs. 13°C for GFL I_K). Steady-state block quantified as f_B decreases with a nonexponential time course (Fig. 7 B). Nitrosothiols have a characteristic absorbance peak at ~330 nm (Arnelle and Stamler, 1995; Le et al., 1997), and because the breakdown reaction of SNDTT does not involve a singly niotrosylated intermediate, this peak provides a relative measure of SNDTT concentration. The exact location of this peak under our conditions is at 333 nm (Fig. 7 C). Breakdown of SNDTT is apparent in the decreasing absorbance at 333 nm (A_{333}) over time (Fig. 7 D). As predicted for an intramolecular mechanism of breakdown, SNDTT concentration decays exponentially, with a time constant of 773 s.

The difference in the time courses of f_B (Fig. 7 B) and A_{333} (Fig. 7 D) is expected, because f_B is not directly proportional to SNDTT concentration. The time course of f_B agrees satisfactorily with the prediction of Scheme III for an exponential decrease in SNDTT with the 773 s time constant observed above (Fig. 7 B, solid curve). Values for K_{d1} (0.33 mM) and K_{d2} (0.07 mM) for this calculation were chosen to match the first f_B data point, while holding the K_{d1}/K_{d2} ratio constant at the value (4.7) determined in Fig. 4 E. Deviation of the data at longer times after synthesis is probably due to measurement of f_B with 250-ms depolarizations, which are too short to permit block to reach steady-state levels for low concentrations of SNDTT.

SNDTT Binding Determinants

Several facts suggest that the molecular interaction between SNDTT and the open channel is unique. SNDTT, in contrast to conventional open-channel blockers, lacks fixed charge and has little hydrophobic structure. Moreover, its four carbons (vs. 16 for C_{10} and 27 for verapamil, Fig. 1) each have a polar functional group attached. Most importantly, the ineffectiveness of DTT (Figs. 2 and 3) indicates that the polar nitrosothiol groups are critical to the blocking action of SNDTT.

Synthesis conditions used thus far favor the complete nitrosylation of both thiols on DTT, and the breakdown of SNDTT does not involve a singly nitrosylated intermediate (Arnelle and Stamler, 1995; Le et al., 1997). This raises the question of the relative efficacy of singly nitrosylated DTT (referred to henceforth as SN_1DTT) as a channel blocker, and more generally, the question of the minimum structural requirements for block. The bilateral molecular symmetry of SNDTT clearly suggests that the compound might be bifunctional, with each end acting independently as a blocker. In this case, structurally related nitrosylated monothiols would be expected to produce block.

To test this possibility, we synthesized S-nitroso-β-mercaptoethanol (SN-β-ME) and S-nitroso-1-thioglycerol (SN-1-TG), which are essentially truncated versions of SNDTT that lack a second nitrosothiol group. Despite this structural similarity, neither of these compounds shows an appreciable effect on ShBΔ I_K (Fig. 8 A), consistent with the insufficiency of a single nitrosothiol group for SNDTT-like block.

In a second approach to this issue, we directly compared the potency of SNDTT and SN_1DTT. If NO_2 is reacted with a great excess of DTT, the probability is very low that both thiols on a single DTT molecule will be nitrosylated, and the resulting concentration of SN_1DTT will be virtually equal to that of added NO_2 (Le et al., 1997). To this end, we used a 1:10 NO_2/DTT synthesis ratio to preferentially synthesize SN_1DTT, and diluted the product to yield a final concentration of 0.5 mM. A_{333} for 0.5 mM SN_1DTT is half that of 0.5 mM SNDTT (3:1 synthesis ratio), consistent with 1 and 2 nitrosothiol groups per DTT, respectively (Fig. 8 B, panel i).

Effects of SN_1DTT and SNDTT (both at 0.5 mM concentration) on ShBΔ I_K are compared for a single cell in Fig. 8 B (panel ii). SN_1DTT has a negligible effect, whereas SNDTT causes profound block, consistent with a critical necessity for the dinitrosothiol motif. The ~10% reduction of I_K in the left panel of Fig. 8 B (panel ii) is likely due to the small amount of SNDTT predicted to be present at the 1:10 synthesis ratio. The impotency of SN_1DTT is not due to markedly faster breakdown: under our experimental conditions A_{333} decreases with a time constant of ~650 s (not illustrated), not markedly different than that of SNDTT (~770 s).

Variation of the NO_2/DTT synthesis ratio (r) was also performed at intermediate values where significant amounts of both SN_1DTT and SNDTT are expected to exist. Fig. 8 C illustrates results from an experiment in which the DTT concentration was kept constant at 1 mM, and r was varied between 0 and 5. Values of $r < 2$ are obviously insufficient to nitrosylate both thiol groups on each DTT molecule, and in the absence of strong positive cooperativity, should result in some amount of SN_1DTT. A_{333} provides a relative measure of the total concentration of nitrosylated thiol groups in the resulting product, and this quantity varies linearly with r up to $r = 2$, where it abruptly saturates (Fig. 8 C, i, □). This relationship is consistent with all NO_2 reacting with available thiol groups until NO_2 is in excess ($r > 2$), at which point both thiols on all DTT molecules are nitrosylated.

Effects of these products on ShBΔ I_K at +20 mV are illustrated in Fig. 8 C (panel ii), where it can be seen that potency also saturates at $r = 2$. The relationship between f_B (●) and r is plotted in Fig. 8 C (panel iii).

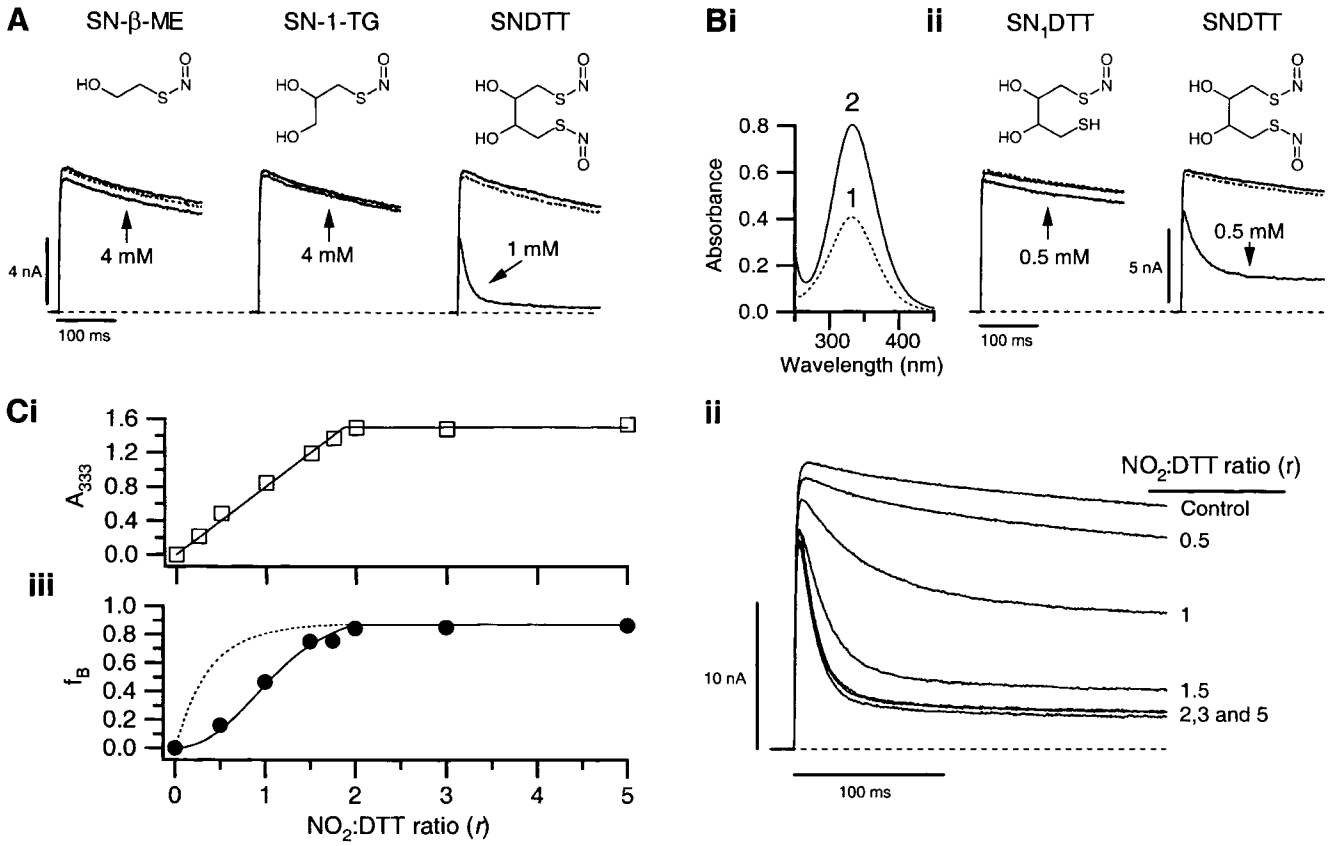

FIGURE 8. The dinitrosothiol motif is critical for block. (A) Nitrosylated monothiols have no effect. S-nitroso-β-mercaptoethanol (SN-β-ME), S-nitroso-1-thioglycerol (SN-1-TG), and SNDTT were individually bath-applied to the same cell at the indicated concentrations with intervening washes. For each compound, I_K at +40 mV is shown before application (unmarked), in the presence of the compound (arrow), and after washout (dotted). A structure for each compound is displayed above the respective set of traces. (B) Essentially pure singly nitrosylated DTT (SN_1DTT) has no effect. SN_1DTT was synthesized (see MATERIALS AND METHODS) using a 1:10 NO_2/DTT synthesis ratio and diluted to 0.5 mM. Doubly nitrosylated DTT (SNDTT) was synthesized using a 3:1 ratio. (panel i) Absorbance spectra for 0.5 mM SN_1DTT ("1"; dashed line) and SNDTT ("2"; solid line), acquired two minutes post-synthesis. (panel ii) Effect of SN_1DTT and SNDTT on ShBΔ I_K at +40 mV. Markings are as in A. Structures for both compounds are shown above their respective set of traces. (C) Effect of SNDTT at intermediate synthesis ratios is consistent with only the di-nitroso form being active. DTT was nitrosylated with NO_2/DTT synthesis ratios (r) between 0 and 5, and these stocks were diluted so that the concentration of total DTT (i.e., reacted + unreacted) remained constant at 1 mM. (panel i) Absorbance at 333 nm (A_{333}; □) was used as a relative measure of the total concentration of nitrosothiol groups in these products. The solid line is a fit to a saturating linear relationship where the saturation point had a best fit value of $r = 1.9$, close to the predicted value of 2.0 for this reaction. (panel ii) I_K at +20 mV is illustrated for the products of several synthesis ratios. Application of each product was bracketed with washouts, and traces were scaled for small (≤10%) variation in control I_K as described in Fig. 4. (panel iii) Steady-state relationship between fraction of channels blocked (f_B; ●; measured at 250 ms from experiment in panel ii) and the NO_2/DTT synthesis ratio. Smooth curves are predictions of Scheme III based on the assumption that nitrosylation occurs randomly (i.e., nitrosylation of one thiol on DTT is insensitive to whether the other thiol is nitrosylated). Under this assumption, the concentrations of [SNDTT] and [SN_1DTT] are directly related to the probability $P = r/2$ that a given thiol group is nitrosylated. The solid line represents the case where only SNDTT blocks:

$$[S] = [SNDTT] = \begin{cases} (1\text{ mM})(r/2)^2, & r < 2 \\ 1\text{ mM}, & r \geq 2. \end{cases}$$

The quantity $(r/2)^2$ in this equation is the probability that both thiols on a given DTT molecule are nitrosylated. The dotted line represents the case in which SNDTT and SN_1DTT are equipotent:

$$[S] = [SN_1DTT] + [SNDTT] = \begin{cases} (1\text{ mM})(1-(1-r/2)^2), & r < 2 \\ 1\text{ mM}, & r \geq 2. \end{cases}$$

with the quantity $(1-(1-r/2)^2)$ being equal to the probability that one or two thiols on a given SNDTT molecule are nitrosylated. The factor "1 mM" is the total concentration of DTT (reacted + unreacted), and therefore, the saturated value for [S]. The f_B versus r relationship for each case was generated by substituting the above equations into Eq. 3 in RESULTS. Values for K_{d1} (1.00 mM) and K_{d2} (0.21 mM) were chosen to reproduce the observed saturated level of f_B while keeping the K_{d1}/K_{d2} ratio constant at the value (4.7) determined in Fig. 4 E.

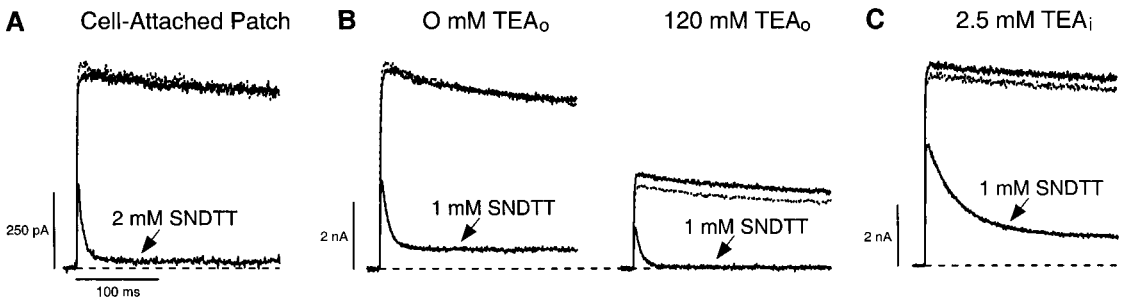

FIGURE 9. SNDTT is membrane-permeant and blocks from the inside. (A) Effect of bath-applied SNDTT on ShBΔ I_K in a cell-attached patch. I_K at +40 mV was acquired before SNDTT application (unmarked), in the presence of 2 mM SNDTT (arrow), and after washout (dotted). Bath solution consisted of normal 20 mM K^+ external solution with an additional 120 mM K^+ (140 mM K^+ total), which replaced sodium on an equimolar basis. The patch pipet contained normal 20 mM K^+ external. (B) External TEA (TEA_o) has no effect on the kinetics of SNDTT block. Block of whole-cell ShBΔ I_K at +40 mV by 1 mM SNDTT was observed in the absence (left) and presence (right) of 120 mM TEA_o (replacing Na on an equimolar basis). Markings are as in A. Least-squares single exponential fits to the decay of I_K in the presence of SNDTT are superimposed on the respective traces, and have τ_{block} values of 8.4 ms (0 mM TEA_o) and 7.8 ms (120 mM TEA_o). (C) Internal TEA (TEA_i) slows the kinetics of SNDTT block. I_K at +40 mV was acquired with 2.5 mM TEA in the patch pipet. Markings are as in A. A least-squares single exponential fit to the decay of I_K in the presence of SNDTT is superimposed on the trace, and has a τ_{block} of 40.8 ms.

These data are well fit by the sigmoidal solid curve, which is the prediction of Scheme III with SNDTT being the only active species. As described in the legend, the dotted curve is the Scheme III prediction for the case where SNDTT and SN_1DTT are equipotent, and the fit is obviously very poor. This analysis reinforces the idea SN_1DTT has an extremely low affinity for binding to the open channel and that virtually all observed block is due to SNDTT.

Binding Site

Results of whole-cell experiments described thus far have demonstrated the effectiveness of bath-applied SNDTT. When included in the pipet at concentrations up to 3 mM in whole-cell experiments, SNDTT is ineffective (data not illustrated). This pattern is similar to that for tertiary amines such as verapamil (DeCoursey, 1995; Rauer and Grissmer, 1996) and methadone (Horrigan and Gilly, 1996; our unpublished data) which when bath-applied, reach their internal binding site by permeating the membrane in their neutral, unprotonated form. In whole-cell experiments, inclusion of these blockers in the pipet results in ineffective concentrations at the inner surface of the cell membrane because the pipet acts as a point source of a membrane-permeant compound.

To assess the membrane permeability of SNDTT, we tested bath-applied SNDTT on ShBΔ channels in a cell-attached patch. In this configuration, SNDTT must pass through the membrane at least once to gain access to the channels under study. As can be seen in Fig. 9 A, bath-application of 2 mM SNDTT in this configuration produces the signature effects seen in whole-cell experiments.

Because SNDTT is membrane permeant, its effectiveness when bath-applied does not distinguish between an external versus internal binding site, as the cytoplasmic concentration of SNDTT should equilibrate with the bath concentration. Therefore, a second approach was necessary to determine the sidedness of SNDTT block. We reasoned that if SNDTT directly occludes the channel pore, its binding site would likely overlap with that of either internal or external TEA. TEA is known to have distinct binding sites at both the external and internal ends of the Kv1 channel selectivity filter (MacKinnon and Yellen, 1990; Kirsch et al., 1991; Yellen et al., 1991; Heginbotham and MacKinnon, 1992), and because it is membrane impermeant, can be confined to either the extracellular or intracellular side of the membrane by inclusion in the bath or pipet respectively in whole-cell experiments. If the transient presence of bound TEA temporarily prevents a process from proceeding (i.e., "competition"), the macroscopic kinetics of that process will be slowed by a factor equal to the degree of channel block by TEA (Grissmer and Cahalan, 1989; Douglass et al., 1990; Grissmer et al., 1990; Choi et al., 1991). This approach has been used to show that the binding site of tertiary amine open-channel blockers overlaps with that of internal TEA (Catacuzzeno et al., 1999) and tetrapentylammonium (Snyders and Yeola, 1995).

Fig. 9 B illustrates an experiment in which the kinetics of ShBΔ block by SNDTT were observed in a single cell both in the absence and presence of 120 mM external TEA (TEA_o). This concentration of TEA blocks ~50% of channels, but has a negligible effect on the kinetics of block by 1 mM SNDTT.

Competition between SNDTT and internal TEA (TEA_i) was tested by examining the kinetics of block of ShBΔ by SNDTT in cells with 2.5 mM TEA in the pipet, and data from a representative cell is shown in Fig. 9 C. Block by SNDTT proceeds about fivefold more slowly in these cells (τ_{block} = 40.8 ± 8.4; mean ± SEM for four cells) than in control cells with 0 TEA_i (τ_{block} = 8.3 ± 0.8

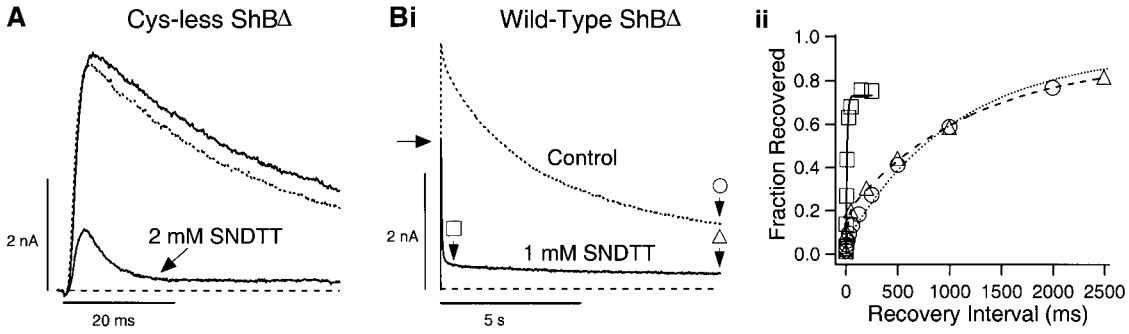

FIGURE 10. SNDTT block does not require channel cysteines, and is not simply an acceleration of endogenous C-type inactivation. (A) SNDTT blocks a *Shaker* mutant lacking all cysteine residues. Cys-less ShBΔ, in which all six wild-type cysteines have been substituted by serine, valine, or alanine (see MATERIALS AND METHODS), was transiently expressed in HEK 293 cells. I_K at +40 mV is shown before the application of SNDTT (unmarked), in the presence of 2 mM SNDTT (arrow), and after washout (dotted). (B) SNDTT block is distinct from inactivation. This experiment used ShBΔ with no additional mutations (see MATERIALS AND METHODS) expressed in the Sf9 insect cell line. (panel i) Block versus C-type inactivation. Whole-cell I_K during a 10-s depolarization to +40 mV is illustrated before (dotted) and after (solid) the addition of 1 mM SNDTT. Peak I_K in the presence of SNDTT is indicated with an arrow. (panel ii) Recovery from block versus inactivation. Fraction recovered was calculated as in Fig. 3 from two-pulse recovery protocols initiated at the times indicated by the symbols in panel i. After a 10-s pulse in the absence of SNDTT (○), recovery at −80 mV is well described by a single exponential with τ = 1,055 ms (dotted line). After a 250-ms depolarization in the presence of 1 mM SNDTT (□), recovery is much faster (τ = 12 ms, solid line). After a 10-s depolarization in the presence of 1 mM SNDTT (△), however, recovery is primarily slow. A double exponential fit (dashed line) reveals a major component (75% of amplitude) with τ = 1,175 ms, and a minor component (25%) with τ = 15 ms.

ms). Based on a K_d of 0.7 mM for internal TEA (Yellen et al., 1991), 2.5 mM TEA_i should reduce ShBΔ I_K by 4.6-fold, a value close to that for the observed slowing. Although a rigorous test of an exclusive competition mechanism would require comparison of $\tau_{TEA}/\tau_{control}$ versus $I_{control}/I_{TEA}$ values for a range of TEA concentrations, our data are consistent with the interference of internal TEA with SNDTT binding, and point to the existence of an internal binding site for SNDTT that either overlaps that of TEA, or is inaccessible when TEA is bound.

Mechanism of Action

Although the reversibility and concentration dependence of ShBΔ block by SNDTT seem consistent with noncovalent block, possibly by two SNDTT molecules, we explored several conceivable alternatives. First, we considered the possibility that SNDTT has a unique ability among tested nitrosothiols to transnitrosate a channel cysteine residue, and that this reaction underlies the observed activity of SNDTT. To assess the role of cysteines in SNDTT block, we took advantage of the previously characterized ShBΔ mutant, Cys-less ShBΔ, in which all wild-type cysteines have been mutated (Boland et al., 1994; see also MATERIALS AND METHODS). The effect of 2 mM SNDTT on Cys-less ShBΔ is illustrated in Fig. 10 A. Although this channel has unusually fast C-type inactivation, profound state-dependent block by SNDTT is evident in the faster decay of I_K and greatly reduced I_K amplitude. These effects reverse to near completion upon washout. These results demonstrate unambiguously that cysteines in ShBΔ are not required for SNDTT block. Although experiments in this report do not rule out nitrosylation at a residue other that cysteine as the mechanism of SNDTT action, other amino acids are generally considered to be much less reactive (Simon et al., 1996). The ineffectiveness of nitrosylated monothiols (Fig. 8), which presumably would also have the ability to donate an NO group, also argues against channel nitrosylation as the mechanism of block.

In light of the qualitatively similar effects of open-channel block and C-type inactivation on I_K (i.e., an exponential decrease in I_K), one conceivable mechanism of SNDTT action is through an enhancement of endogenous C-type inactivation rather than a direct occlusion of the pore. Two lines of evidence argue against this possibility. First, the rate and apparent affinity of SNDTT block for individual Kv1 subfamily members do not correlate with endogenous rates of C-type inactivation (see Fig. 11). Second, results of a two-pulse recovery experiment suggest that inactivation can proceed independently of block (Fig. 10 B). Wild-type ShBΔ (expressed in the Sf9 insect cell line) was used for this experiment because of the larger fraction of channels that undergo C-type inactivation in comparison to the T449V mutant used elsewhere in this study. At +40 mV, these channels inactivate to ~70% completion with a $\tau_{inac} \approx 3.5$ s (Fig. 10 B, panel i, dotted trace). Recovery from this inactivation proceeds slowly at −80 mV (Fig. 10 B, panel ii, ○; τ_{rec} = 1,055 ms).

The effect of 1 mM SNDTT on wild-type ShBΔ is shown in Fig. 10 B (panel i, solid trace). The time course of recovery from this block at −80 mV depends on pulse length (Fig. 10 B, panel ii). After a brief depolarization (250 ms) during which few (control) channels inactivate, recovery from SNDTT block is fast (□;

τ_{rec} = 12 ms). However, after a 10-s depolarization, during which 70% of channels inactivate in the control trace, recovery from SNDTT block is primarily slow (△; τ_{slow} = 1,175 ms) and closely matches the time course of recovery from inactivation. A minor fast component (τ_{fast} ~15 ms) presumably represents recovery of blocked channels that have not inactivated. This result suggests that C-type inactivation can proceed while channels are blocked by SNDTT, and is thus a process distinct from SNDTT block.

This observed rate of recovery from SNDTT block for wild-type ShBΔ in Sf9 cells is much faster than that reported above (Fig. 3) for ShBΔ T449V, C301S, C308S in HEK 293 cells. Factors other than amino acid differences may contribute to this discrepancy, including differences in the composition of physiological solutions, and differences in cellular environment. The relative contributions of such factors are unclear.

Kv Subfamily Specificity

Results in Fig. 2 demonstrate that SNDTT displays specificity for Kv channels over Na^+ and Ca^{2+} channels. Within the Kv family of channels, block by SNDTT displays a high degree of specificity for the Kv1 subfamily (Fig. 11). Both ShB and the channel proposed to underlie I_K in GFL cells (SqKv1A; Rosenthal et al., 1996) belong to this subfamily. In addition to results with these channels, we confirmed that SNDTT blocks the mammalian Kv1 members rKv1.1–1.6 (Fig. 11, left and center columns). 1 mM SNDTT induces reversible, time-dependent block of I_K in each Kv1 member, although the kinetics and degree of block show some variation. SNDTT was also tested on one member of the Kv2, 3, and 4 subfamilies, but time-dependent I_K block was not evident in any of these (Fig. 11, right column). Kv2.1, 3.1b, and 4.2 instead show small, time-independent reductions in I_K amplitude that were not reversible by solution washout. Such small irreversible reductions could conceivably be due to long-lived nitrosylation of channel cysteines, however this effect was not studied further. The qualitatively different effect of SNDTT on Kv1 versus Kv2, 3 and 4 channels indicates that a high degree of specificity exists for this small, structurally simple compound.

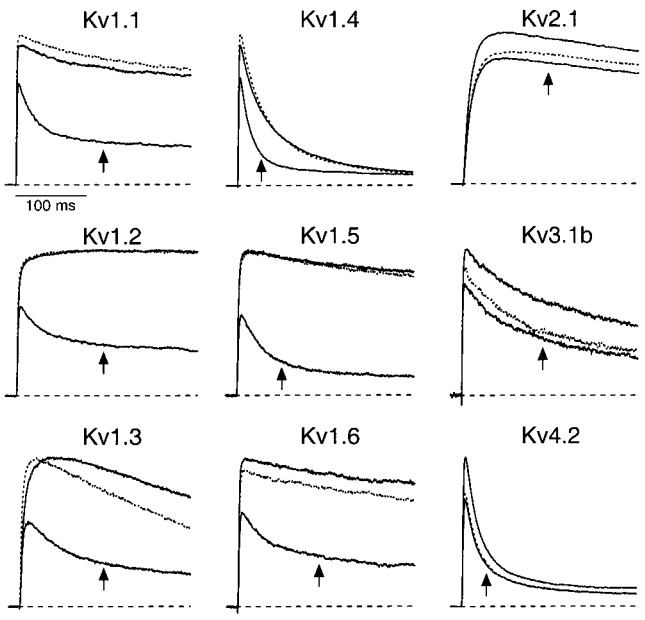

FIGURE 11. SNDTT is selective for Kv1 subfamily channels. The indicated rat Kv channels were transiently expressed in HEK 293 cells. For each channel, whole-cell I_K at +40 mV was assayed before the addition of SNDTT (unmarked), in the presence of 1 mM SNDTT (arrow), and after SNDTT washout (dotted). Sensitivity to SNDTT was assayed in at least two cells expressing each channel type. Although concentration dependence was confirmed for each Kv1 subfamily member, detailed dose–response curves were not obtained. Note that SNDTT causes reversible, time-dependent block only in Kv1 subfamily channels. Peak control I_K amplitudes in nA for each panel were as follows: Kv1.1 = 8.1, Kv1.2 = 7.5, Kv1.3 = 7.3, Kv1.4 = 13.6, Kv1.5 = 6.1, Kv1.6 = 5.0, Kv2.1 = 13.3, Kv3.1b = 0.9, and Kv 4.2 = 16.9.

DISCUSSION

This paper describes the block of open Kv1 channels by SNDTT. The most important findings relating our work to the extensive literature on open-channel block produced by quaternary ammonium and tertiary amine compounds are as follows. First, SNDTT appears to block K^+ channels with a 2:1 stoichiometry; all conventional open-channel blockers show a 1:1 interaction. Second, SNDTT has a novel structure for a K^+ channel blocker. It is neither an amine nor hydrophobic, and has two nitrosothiol groups, both of which are critical for activity. Therefore, SNDTT is likely to interact with the channel in a chemically unique way. Third, SNDTT, despite a lack of fixed charge, blocks channels with a voltage dependence of comparable magnitude, but opposite sign, to that of conventional open-channel blockers. Fourth, SNDTT shows a high degree of specificity for the Kv1 subfamily of voltage-gated K^+ channels.

SNDTT Shows a Novel 2:1 Stoichiometry

Knowledge of the precise stoichiometry of the interaction between SNDTT and the channel is fundamental to the interpretation of physiological results, and the 2:1 value proposed in this study is novel for a blocker of open K^+ channels. Arguments against a 1:1 interaction are based on conventional analysis of dose–response data that indicate neither 1:1 nor 2:1 binding (for Scheme I) adequately fits the experimental data. Although a reasonable fit can be obtained for 1.4 SNDTT molecules/channel, this notion is physically nonsensical.

Alternatively, relaxing the simultaneous binding constraint for two blockers in Scheme I leads to more plau-

sible, sequential-binding models in which either two SNDTT molecules are necessary to block the channel (Scheme II) or in which one molecule is sufficient (Scheme III). Of the two, Scheme III provides a demonstrably better fit of dose–response data. For this reason, we are inclined to accept Scheme III at the present time, and use it to predict various other features of SNDTT block in this paper.

Potential Errors in Determining Stoichiometry. Because the 2:1 stoichiometry for a K^+ channel-blocker is novel, it is important to consider artifacts that might impact its accurate determination. Errors in the calculation of f_B for a given concentration of SNDTT could stem from either inaccuracies in the concentration of applied SNDTT or artifacts involved with I_K measurements. Because some breakdown of SNDTT inevitably takes place before any measurements can be made, concentration is obviously a concern. Breakdown of SNDTT occurs by an intramolecular reaction, and the time constant of breakdown in our experiments as monitored by A_{333} is predictably independent of starting concentration (not illustrated). The shape of dose–response relationships, therefore, will be preserved for determinations of f_B made at matched times post-synthesis.

Inaccuracies in I_K measurement represent another potential source of error that could alter the shape of the dose–response curve. Small amounts of nonlinear leak current or endogenous I_K in HEK 293 cells (Yu and Kerchner, 1998) that were insensitive to SNDTT would disproportionately affect determinations of f_B at high concentrations of SNDTT, where this current might represent a significant fraction of I_K. This would result in artificially low f_B values and reduce the slope of the dose–response relationship at high concentrations, the region where we find a slope that approaches $N = 2$.

Similarly, voltage errors due to series resistance would also lead to an underestimate of f_B that would be more serious at higher concentrations, where differences in I_K (and consequently actual voltage) in the absence and presence of SNDTT would be maximal. Again, this would act to reduce the steepness of the dose–response curve. Series resistance errors in the present study, however, were small enough that correction of control I_K did not significantly change the dose–response data or the voltage dependence of block (not illustrated; see MATERIALS AND METHODS).

A final consideration concerns the form of SNDTT used in the present study, which is a racemic mix of two enantiomers (D-SNDTT and L-SNDTT) based on the corresponding stereoisomers of DTT (D-DTT and L-DTT; Cleland, 1964). These stereoisomers could have distinct binding properties. A scheme in which two blocking species with distinct affinities compete for a single binding site, however, is still described by Scheme I with $N = 1$, and the poor fit of Scheme I to our data is therefore not an artifact of this complexity (see APPENDIX). Moreover, as also shown in the APPENDIX, the ability to distinguish between Schemes II and III is also not affected by the presence of two isomers with distinct K_d values. Nevertheless, the numerous possibilities for occupancy, cooperativity, and temporal sequence for combinations of two different isomers make the overall situation potentially very complex, and values determined here for K_{d1} and K_{d2} undoubtedly represent more complex functions of the numerous dissociation constants necessary to fully describe this situation (see APPENDIX). Future experiments with individual stereoisomers will be necessary for an accurate determination of steady-state and kinetic parameters for Scheme III.

Chemical Interaction of SNDTT and the Open K^+ Channel

Given the enormous sizes of the blockers that a potassium channel cavity can apparently accommodate, it seems reasonable that the small size of SNDTT can allow occupancy by two molecules at the same time. This possibility is even more attractive when the twofold symmetry of SNDTT and the fourfold symmetry of Kv channels are considered. Each of two SNDTT molecules could have virtually identical contacts with two adjacent channel subunits, and interactions between the two bound SNDTT molecules might also be relevant.

Binding Determinants and Nature of Interaction. K_d as defined in Eq. 1 is related to the standard free energy change for the binding reaction by:

$$\Delta G^0 = RT \ln K_d.$$

For block by ShBΔ channels by decyltriethylammonium (C_{10}, $K_d = 0.75$ μM; Choi et al., 1993), ΔG^0 is about −8 kcal/mol.

The equivalent relation for Scheme III is given by:

$$\Delta G^0_{total} = \Delta G^0_1 + \Delta G^0_2 = RT \ln (K_{d1} K_{d2}),$$

where the subscripts 1 and 2 refer to the first and second binding events, respectively. Values for K_{d1} and K_{d2} obtained in the fitting of dose–response data (Fig. 4) yield a total binding energy of about −9.5 kcal/mol for a pair of SNDTT molecules.

Although the total binding energies for SNDTT and C_{10} are thus comparable, the distinct chemical nature of the two compounds indicates that interactions with the channel are likely to be quite different in each case. For TEA derivatives with progressively longer n-alkyl chains, each additional methylene group contributes ∼0.5–0.7 kcal/mol of additional energy to binding (Armstrong, 1969; Choi et al., 1993). Thus, the energy of this hydrophobic interaction appears to be rather evenly distributed over the entire structure of these compounds. The same generalization presumably ap-

plies to even larger hydrophobic blockers like those depicted in Fig. 1 (Longobardo et al., 1998). Given the diversity of such structures that block Kv1 channels with roughly the same potency, it is difficult to imagine that the relevant hydrophobic interactions are highly specific for either the exact structure of hydrophobic moieties or their precise spatial arrangement. In contrast, the smaller size of one or two SNDTT molecules implies that a binding energy of similar magnitude is likely to be focused in a small number of more specific interactions with the channel.

What might the nature of these interactions be? The structure of SNDTT suggests they are unlikely to be hydrophobic. In the absence of evidence for covalent modification of channels by SNDTT, hydrogen bonding must be seriously considered. The estimated $\Delta G^0_{\text{total}}$ for SNDTT binding of −9.5 kcal/mol is roughly equal to the energy of several weak hydrogen bonds, although $\Delta G^0_{\text{total}}$ will reflect competition with water molecules for bonding. Each SNDTT molecule has four polar groups that could conceivably be involved in hydrogen bonding with the channel, and the likelihood that two SNDTT molecules bind to a single channel must also be taken into account. Ineffectiveness of DTT argues that the two backbone hydroxyls are not likely to be primary binding determinants, and points to a critical involvement of the nitrosothiol groups. For example, the oxygen atom on these highly polar groups could act as a hydrogen bond acceptor in an interaction with a donor group on the channel. Unusually high potency of conventional open-channel blockers that contain polar oxygen–containing groups 3–4 carbons away from the charged nitrogen has been previously noted (Swenson, 1981), suggesting that polar interactions may be of more general relevance as well.

Cooperativity. In Scheme III for SNDTT binding, the dissociation constant for binding of the first SNDTT molecule (K_{d1}) is about fivefold higher than that for the second molecule (K_{d2}). This positive cooperativity is equivalent to a stabilization of the second binding event by ∼1 kcal/mol, and it is attractive to speculate that this energy derives from hydrogen bonding between the backbone hydroxyl groups of the two SNDTT molecules. Alternatively, these backbone hydroxyls could actively interact with the channel, and nitrosylation of DTT might favor an overall conformation of SNDTT that presents the backbone hydroxyls in a critical manner. In this case, polar interactions involving the nitrosothiol groups of SNDTT might provide the basis for the observed cooperativity.

Binding Site. The state dependence of SNDTT block as well as the competition for binding with TEA suggest that either SNDTT binds in the K^+ channel cavity, or that access to its site involves passage through the cavity. The lining of this cavity (S6 residues) is largely hydrophobic (Doyle et al., 1998), consistent with the primarily hydrophobic determinants for the binding of QA ions (Armstrong, 1969, 1971; French and Shoukimas, 1981; Swenson, 1981; Choi et al., 1993). Position 469 in the S6 helix of ShB has a particularly strong influence on the binding of QA ions. Substitution of more hydrophobic amino acids at this position increases the affinity for long-chain QA ions (Choi et al., 1993). Similarly, more hydrophobic residues at the equivalent position in Kv1.5 increase the affinity for the tertiary amine quinidine (Yeola et al., 1996).

Of the amino acids thought to line the *Shaker*B cavity, threonine at position 469 stands out as a polar residue. The hydroxyl-containing side chain of this residue, therefore, provides an attractive candidate for the aforementioned hydrogen bond donor required to interact with SNDTT. Hydrogen bonding between SNDTT and this residue might also partially explain the selectivity of SNDTT for Kv1 channels: threonine is apparently conserved in all Kv1 α-subunits, whereas Kv2.1 and Kv4.2 have a hydrophobic valine at this position. However, Kv3.1b, like Kv1 channels, has a threonine at this position, and it is therefore unlikely that this position alone is the sole determinant of SNDTT affinity. Several polar residues located at the inner end of the P-loop of Kv channels (ShB M440, T441, and T442) are also exposed to the cavity (Doyle et al., 1998) and could also be candidates. Binding of TEA to ShB is extremely sensitive to mutations at residues 440 and 441 (Yellen et al., 1991; Choi et al., 1993), and the observed inhibition of SNDTT binding by TEA suggests that these residues may also interact with SNDTT.

Voltage Dependence of SNDTT Binding

Voltage dependence of block produced by SNDTT is surprising given the absence of fixed charge on SNDTT. In the case of Kv block by QA ions and tertiary amines, this phenomenon has been universally interpreted in terms of the binding of the charged blocker within the voltage field across the cell membrane. Our results demonstrate that properties other than fixed charge can contribute to the observed voltage dependence. In the case of SNDTT, voltage dependence of steady-state block is similar in magnitude to that for Kv block by QA ions, but opposite in sign: more positive potentials lower the affinity for SNDTT.

Interference of internal TEA with SNDTT binding strongly suggests that SNDTT, like TEA, binds within the membrane voltage field. One possible source of voltage dependence for SNDTT binding is the dipole moment associated with the nitrosothiol groups. Positive voltages may destabilize binding by influencing the orientation of these dipoles, thereby disrupting highly directional hydrogen bonds between SNDTT and the channel. Alternatively, conformational changes in the channel could

underlie the voltage dependence. At the voltages where steady-state block was analyzed (≥0 mV), however, g_K is essentially saturated, so such conformation changes would not normally contribute to changes in open probability. Finally, the voltage dependence might also be due to interaction of SNDTT with K^+ ions in the pore, although this effect obviously cannot be attributed to simple electrostatic interactions between point charges.

Selectivity

Selectivity of SNDTT for one molecular subtype of Kv channels (Kv1) does not seem surprising, given the necessity that interactions between SNDTT and the channel are fewer in number and of higher energy than those for conventional open-channel blockers. In this capacity, SNDTT should be valuable as a pharmacological probe for Kv channels in native systems. Furthermore, SNDTT and structural variants may provide new inroads into the design of pharmaceuticals with refined specificities. Members of the large Kv channel family are critical determinants of excitability in many cell types (Rudy, 1988), making block of these channels a fertile area for drug development. This widespread distribution, however, will require high specificities for target channels.

APPENDIX

Coefficients for Schemes II and III Dissociation Constants

Coefficients preceding K_{d1} and K_{d2} in Schemes II and III result from the following statistical considerations. Because the first binding step in both schemes represents the occupancy of either of two intrinsically identical sites, the apparent forward rate for this event will be twice that of either site in isolation, or $2\kappa_1$. With one site occupied, binding can only occur at the one remaining site, and the coefficient of the corresponding forward rate κ_2 is simply unity. A similar argument can be made for the reverse rates. In a channel with two blocker molecules bound, either site can lose its blocker, and the rate at which this event occurs is twice the rate of either site alone, or $2\lambda_2$. The coefficient for the loss of the remaining blocker molecule (λ_1) will be unity. The apparent dissociation constant for the first transition of both schemes is therefore $\lambda_1/2\kappa_1 = 0.5K_{d1}$, and the apparent dissociation constant for the second transition is $2\lambda_2/\kappa_2 = 2K_{d2}$. A similar treatment is found in Colquhoun and Hawkes (1995) for nicotinic acetylcholine receptors with two agonist binding sites.

Behavior of Schemes II and III at Concentration Extremes

A useful simplification for Schemes II and III concerns the behavior of the respective equilibrium equations at high and low blocker concentrations. As can be seen from Eq. 2 in RESULTS, Scheme II is approximated by a Scheme I: $N = 2$ curve at low concentrations and a Scheme I: $N = 1$ curve at high concentrations:

$$f_B \approx \begin{cases} \left(1 - \dfrac{[S]^2}{K_{d1}K_{d2}}\right)^{-1}, & [S] < \dfrac{K_{d1}}{2} \\ \left(1 - \dfrac{[S]}{2K_{d2}}\right)^{-1}, & [S] > \dfrac{K_{d1}}{2}. \end{cases}$$

$K_{d1}/2$ represents the value around which the transition between these equations will occur, and is found by solving for the intersection of the upper and lower equations.

For Scheme III (Eq. 3; see RESULTS), the opposite relationship is true:

$$f_B \approx \begin{cases} \left(1 - \dfrac{[S]}{\frac{1}{2}K_{d1}}\right)^{-1}, & [S] < 2K_{d2} \\ \left(1 - \dfrac{[S]^2}{K_{d1}K_{d2}}\right)^{-1}, & [S] > 2K_{d2}. \end{cases}$$

At low concentrations, Scheme III follows a Scheme I: $N = 1$ binding curve, and at higher concentrations, follows a Scheme I: $N = 2$ binding curve.

Simplification of Scheme III was used in our experiments on the voltage dependence of SNDTT block with the following rearrangement for the ratio of blocked to open channels, B/O:

$$B/O = ((1/f_B) - 1)^{-1}.$$

For $[S] > 2K_{d2}$:

$$B/O = \frac{[S]^2}{K_{d1}K_{d2}}.$$

Schemes for Two Stereoisomers with Different Affinities

The D and L stereoisomers of SNDTT, present in equal amounts in our experiments, may have different dissociation constants. It is demonstrated here that this possibility does not affect our ability to distinguish between binding mechanisms represented by Schemes I, II, and III. That is, binding curves for schemes "expanded" to account for the presence of two stereoisomers assume the exact shapes of their simpler counterparts, and therefore will provide fits of identical quality to SNDTT dose–response data.

Scheme IV represents Scheme I for $N = 1$, expanded to account for competition for a single binding site by equimolar amounts of D and L isomers with different affinities:

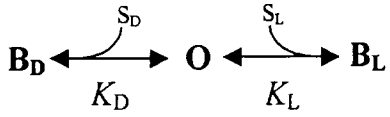

(SCHEME IV)

In this scheme, **O** represents an unliganded channel, $\mathbf{B_D}$ represents a channel blocked by isomer S_D with dissociation constant K_D, and $\mathbf{B_L}$ represents a channel blocked by blocker S_L with dissociation constant K_L. Note that the lowercase "d" subscript used thus far in "K_d" refers generally to "dissociation," whereas a capital "D" will be used to denote the specific dissociation constant for the D isomer. When both isomers are present at concentration [S]/2 (as would be the case for a racemic mix where each isomer makes up half of the total), the solution for f_B is:

$$f_B = \frac{B_D + B_L}{O + B_D + B_L} = \left(1 - \frac{2}{\left(\frac{1}{K_D} + \frac{1}{K_L}\right)[S]}\right)^{-1},$$

which is identical in form to that for Scheme 1 with $N = 1$, and:

$$K_d = 2\left(\frac{1}{K_D} + \frac{1}{K_L}\right)^{-1}.$$

Scheme I for $N = 2$ can also be expanded to take into account the presence of different stereoisomers:

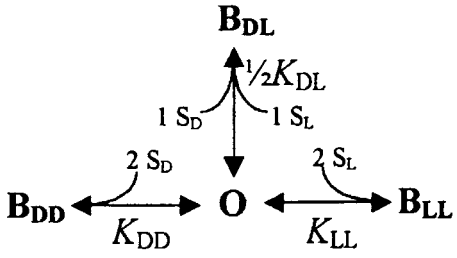

(SCHEME V)

In Scheme V, either two molecules of the D isomer, two of L, or one of each bind simultaneously (a constraint of Scheme I) to form blocked states $\mathbf{B_{DD}}$, $\mathbf{B_{LL}}$, and $\mathbf{B_{DL}}$ respectively. The coefficient of 1/2 preceding K_{DL} is statistical in origin: by the binomial formula, combinations of one D and one L isomer are twice as likely as a pair of D (or L) isomers. The equilibrium equation for this scheme:

$$f_B = \frac{B_{DD} + B_{LL} + B_{DL}}{O + B_{DD} + B_{LL} + B_{DL}} = \left(1 - \frac{4}{\left(\frac{1}{K_{DD}} + \frac{1}{K_{LL}} + \frac{1}{K_{DL}}\right)[S]^2}\right)^{-1},$$

is identical in form to that for Scheme 1 (Eq. 1) with $N = 2$, and

$$K_d = 4\left(\frac{1}{K_{DD}} + \frac{1}{K_{LL}} + \frac{2}{K_{DL}}\right)^{-1}.$$

The expanded versions of Schemes II and III preserve the salient features of their simpler counterparts: in Scheme VI, only channels with two SNDTT molecules bound are nonconducting, whereas in Scheme VII, one SNDTT molecule (of either isomer) is sufficient for block. As for Schemes II and III, it is assumed that the two binding sites are intrinsically identical (i.e., the order in which the sites are occupied is inconsequential). For both schemes, **B** and **O** indicate blocked and open states respectively, and subscripts indicate the absence (U) or presence of one or two bound SNDTT molecules. For example, subscripts D and DD indicate a channel with one or two molecules of D-SNDTT bound respectively, and DL represents a channel with one molecule each of D-SNDTT and L-SNDTT. Both models feature six total transitions and five independent dissociation constants (the sixth is constrained by microscopic reversibility). Unique affinities of D and L isomers for the unliganded channel are represented (K_{U_D} and K_{U_L}), as well as isomer-specific effects of the first molecule bound on the affinity for the second (K_{D_DD}, K_{L_LL}, K_{D_DL}, and K_{L_DL}):

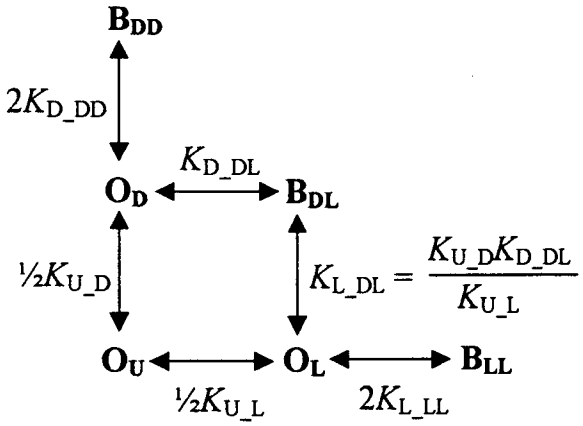

(SCHEME VI)

$$f_B = \frac{B_{DD} + B_{LL} + B_{DL}}{B_{DD} + B_{LL} + B_{DL} + O_U + O_D + O_L} = \left(1 + \frac{A_2}{[S]^2} + \frac{2A_2/A_1}{[S]}\right)^{-1} \quad \text{(A1)}$$

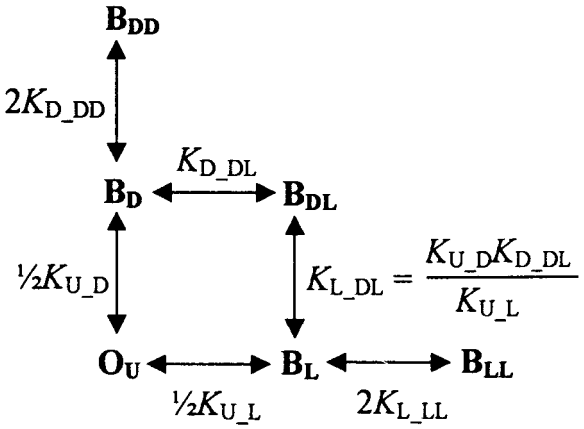

(SCHEME VII)

$$f_B = \frac{B_D + B_L + B_{DD} + B_{LL} + B_{DL}}{O_U + B_D + B_L + B_{DD} + B_{LL} + B_{DL}} = \left(1 + \frac{1}{\frac{[S]}{\frac{1}{2}A_1} + \frac{[S]^2}{A_2}}\right)^{-1}. \quad \text{(A2)}$$

For both schemes, A_1 and A_2 are defined as follows:

$$A_1 = 2(1/K_{U\_D} + 1/K_{U\_L})^{-1}$$

$$A_2 = 4(1/K_{U\_D}K_{D\_DD} + 1/K_{U\_L}K_{L\_LL} + 2/K_{U\_D}K_{D\_DL})^{-1}.$$

Comparison of equilibrium equations for Schemes VI (Eq. A1) and VII (Eq. A2) to those for Schemes II (Eq. 2) and III (Eq. 3), respectively, reveal identical forms where:

$$K_{d1} = A_1,$$

$$K_{d2} = A_2/A_1.$$

Thus, even if D- and L-SNDTT have different dissociation constants, as long as the interaction with the channel involves one of the expanded schemes described above (Scheme IV, V, VI, or VII), fitting the dose–response curves with the simpler Schemes I, II, and III will permit identification of the stoichiometry and sequential nature of SNDTT binding to the channel. Although scenarios where D- and L-SNDTT obey different schemes can be constructed, it would seem unlikely that these isomers interact with K^+ channels by fundamentally different mechanisms.

We thank J.T. Sack, R.W. Aldrich, and S.H. Thompson for comments on the manuscript.

This work was supported by a National Institutes of Health grant (NS-17510) to W.F. Gilly, a National Science Foundation predoctoral fellowship to M.W. Brock, and a National Institutes of Health training grant to Stanford University Neurosciences Program.

Submitted: 19 December 2000
Revised: 16 May 2001
Accepted: 22 May 2001

REFERENCES

Armstrong, C.M. 1969. Inactivation of the potassium conductance and related phenomena caused by quaternary ammonium ion injection in squid axons. *J. Gen. Physiol.* 54:553–575.

Armstrong, C.M. 1971. Interaction of tetraethylammonium ion derivatives with the potassium channels of giant axons. *J. Gen. Physiol.* 58:413–437.

Armstrong, C.M. 1972. Potassium pores of nerve and muscle membrane. *In* Membranes, A Series of Advances. Vol. 2. G. Eisenman, editor. Dekker, New York. 325–358.

Arnelle, D.R., and J.S. Stamler. 1995. NO^+, NO, and NO^- donation by S-nitrosothiols: implications for regulation of physiological functions by S-nitrosylation and acceleration of disulfide formation. *Arch. Biochem. Biophys.* 318:279–285.

Boland, L.M., M.E. Jurman, and G. Yellen. 1994. Cysteines in the *Shaker* K^+ channel are not essential for channel activity or zinc modulation. *Biophys. J.* 66:694–699.

Catacuzzeno, L., C. Trequattrini, A. Petris, and F. Franciolini. 1999. Mechanism of verapamil block of a neuronal delayed rectifier K channel: active form of the blocker and location of its binding domain. *Br. J. Pharmacol.* 126:1699–1706.

Choi, K.L., R.W. Aldrich, and G. Yellen. 1991. Tetraethylammonium blockade distinguishes two inactivation mechanisms in voltage-activated K^+ channels. *Proc. Natl. Acad. Sci. USA.* 88:5092–5095.

Choi, K.L., C. Mossman, J. Aube, and G. Yellen. 1993. The internal quaternary ammonium receptor site of *Shaker* potassium channels. *Neuron.* 10:533–541.

Cleland, W.W. 1964. Dithiothreitol, a new protective reagent for SH groups. *Biochemistry.* 3:480–482.

Colquhoun, D., and A.G. Hawkes. 1995. A Q-matrix cookbook. *In* Single-Channel Recording. B. Sakmann, and E. Neher, editors. Plenum Press, New York. 589–633.

DeCoursey, T.E. 1995. Mechanism of K^+ channel block by verapamil and related compounds in rat alveolar epithelial cells. *J. Gen. Physiol.* 106:745–779.

del Camino, D., M. Holmgren, Y. Liu, and G. Yellen. 2000. Blocker protection in the pore of a voltage-gated K^+ channel and its structural implications. *Nature.* 403:321–325.

Douglass, J., P.B. Osborne, Y.C. Cai, M. Wilkinson, M.J. Christie, and J.P. Adelman. 1990. Characterization and functional expression of a rat genomic DNA clone encoding a lymphocyte potassium channel. *J. Immunol.* 144:4841–4850.

Doyle, D.A., J. Morais Cabral, R.A. Pfuetzner, A. Kuo, J.M. Gulbis, S.L. Cohen, B.T. Chait, and R. MacKinnon. 1998. The structure of the potassium channel: molecular basis of K^+ conduction and selectivity. *Science.* 280:69–77.

French, R.J., and J.J. Shoukimas. 1981. Blockage of squid axon potassium conductance by internal tetra-N-alkylammonium ions of various sizes. *Biophys. J.* 34:271–291.

Gilly, W.F., M.T. Lucero, and F.T. Horrigan. 1990. Control of the spatial distribution of sodium channels in giant fiber lobe neurons of the squid. *Neuron.* 5:663–674.

Gilly, W.F., L.L. Moroz, and R. Gillette. 1995. Redox and nitric ox-

ide (NO)-dependent modulation of potassium channels of squid stellate ganglion neurons. *Recept. Channels.* 21:1832.

Grissmer, S., and M. Cahalan. 1989. TEA prevents inactivation while blocking open K^+ channels in human T lymphocytes. *Biophys. J.* 55:203–206.

Grissmer, S., B. Dethlefs, J.J. Wasmuth, A.L. Goldin, G.A. Gutman, M.D. Cahalan, and K.G. Chandy. 1990. Expression and chromosomal localization of a lymphocyte K^+ channel gene. *Proc. Natl. Acad. Sci. USA.* 87:9411–9415.

Heginbotham, L., and R. MacKinnon. 1992. The aromatic binding site for tetraethylammonium ion on potassium channels. *Neuron.* 8:483–491.

Holmgren, M., M.E. Jurman, and G. Yellen. 1996. N-type inactivation and the S4-S5 region of the *Shaker* K^+ channel. *J. Gen. Physiol.* 108:195–206.

Horrigan, F.T., and W.F. Gilly. 1996. Methadone block of K^+ current in squid giant fiber lobe neurons. *J. Gen. Physiol.* 107:243–260.

Hoshi, T., W.N. Zagotta, and R.W. Aldrich. 1990. Biophysical and molecular mechanisms of *Shaker* potassium channel inactivation. *Science.* 250:533–538.

Kirsch, G.E., M. Taglialatela, and A.M. Brown. 1991. Internal and external TEA block in single cloned K^+ channels. *Am. J. Physiol.* 261:C583–C590.

Le, M., H. Zhang, and G.E. Means. 1997. The decomposition of S-nitrosated dithiols: a model for vicnal nitrosothiols in enzymes. *Bioorg. Med. Chem. Lett.* 7:1393–1398.

Lee, B.S., R.B. Gunn, and R.R. Kopito. 1991. Functional differences among nonerythroid anion exchangers expressed in a transfected human cell line. *J. Biol. Chem.* 266:11448–11454.

Liu, Y., M. Holmgren, M.E. Jurman, and G. Yellen. 1997. Gated access to the pore of a voltage-dependent K^+ channel. *Neuron.* 19: 175–184.

Longobardo, M., E. Delpon, R. Caballero, J. Tamargo, and C. Valenzuela. 1998. Structural determinants of potency and stereoselective block of hKv1.5 channels induced by local anesthetics. *Mol. Pharmacol.* 54:162–169.

Lopez-Barneo, J., T. Hoshi, S.H. Heinemann, and R.W. Aldrich. 1993. Effects of external cations and mutations in the pore region on C-type inactivation of *Shaker* potassium channels. *Receptors Channels.* 1:61–71.

MacKinnon, R., and G. Yellen. 1990. Mutations affecting TEA blockade and ion permeation in voltage-activated K^+ channels. *Science.* 250:276–279.

Malayev, A.A., D.J. Nelson, and L.H. Philipson. 1995. Mechanism of clofilium block of the human Kv1.5 delayed rectifier potassium channel. *Mol. Pharmacol.* 47:198–205.

Rampe, D., B. Wible, A.M. Brown, and R.C. Dage. 1993a. Effects of terfenadine and its metabolites on a delayed rectifier K^+ channel cloned from human heart. *Mol. Pharmacol.* 44:1240–1245.

Rampe, D., B. Wible, D. Fedida, R.C. Dage, and A.M. Brown. 1993b. Verapamil blocks a rapidly activating delayed rectifier K^+ channel cloned from human heart. *Mol. Pharmacol.* 44:642–648.

Rauer, H., and S. Grissmer. 1996. Evidence for an internal phenylalkylamine action on the voltage-gated potassium channel Kv1.3. *Mol. Pharmacol.* 50:1625–1634.

Rosenthal, J.J., R.G. Vickery, and W.F. Gilly. 1996. Molecular identification of SqKv1A. A candidate for the delayed rectifier K channel in squid giant axon. *J. Gen. Physiol.* 108:207–219.

Roux, B., and R. MacKinnon. 1999. The cavity and pore helices in the KcsA K^+ channel: electrostatic stabilization of monovalent cations [see comments]. *Science.* 285:100–102.

Rudy, B. 1988. Diversity and ubiquity of K channels. *Neuroscience.* 25:729–749.

Simon, D.I., M.E. Mullins, L. Jia, B. Gaston, D.J. Singel, and J.S. Stamler. 1996. Polynitrosylated proteins: characterization, bioactivity, and functional consequences. *Proc. Natl. Acad. Sci. USA.* 93: 4736–4741.

Snyders, D.J., and S.W. Yeola. 1995. Determinants of antiarrhythmic drug action. Electrostatic and hydrophobic components of block of the human cardiac hKv1.5 channel. *Circ. Res.* 77:575–583.

Snyders, J., K.M. Knoth, S.L. Roberds, and M.M. Tamkun. 1992. Time-, voltage-, and state-dependent block by quinidine of a cloned human cardiac potassium channel. *Mol. Pharmacol.* 41: 322–330.

Stamler, J.S., D.J. Singel, and J. Loscalzo. 1992. Biochemistry of nitric oxide and its redox-activated forms. *Science.* 258:1898–1902.

Summers, M.D., and G.E. Smith. 1987. A Manual of Methods for Baculovirus Vectors and Insect Cell Culture Proceedures. Texas Agricultural Experiment Station, College Station, TX. 57 pp.

Swenson, R.P., Jr. 1981. Inactivation of potassium current in squid axon by a variety of quaternary ammonium ions. *J. Gen. Physiol.* 77:255–271.

Valenzuela, C., E. Delpon, M.M. Tamkun, J. Tamargo, and D.J. Snyders. 1995. Stereoselective block of a human cardiac potassium channel (Kv1.5) by bupivacaine enantiomers. *Biophys. J.* 69:418–427.

Woodhull, A.M. 1973. Ionic blockage of sodium channels in nerve. *J. Gen. Physiol.* 61:687–708.

Yang, T., C. Prakash, D.M. Roden, and D.J. Snyders. 1995. Mechanism of block of a human cardiac potassium channel by terfenadine racemate and enantiomers. *Br. J. Pharmacol.* 115:267–274.

Yeh, J.Z., and C.M. Armstrong. 1978. Immobilisation of gating charge by a substance that simulates inactivation. *Nature.* 273: 387–389.

Yellen, G. 1998. The moving parts of voltage-gated ion channels. *Quart. Rev. Biophys.* 31:239–295.

Yellen, G., M.E. Jurman, T. Abramson, and R. MacKinnon. 1991. Mutations affecting internal TEA blockade identify the probable pore-forming region of a K^+ channel. *Science.* 251:939–942.

Yeola, S.W., T.C. Rich, V.N. Uebele, M.M. Tamkun, and D.J. Snyders. 1996. Molecular analysis of a binding site for quinidine in a human cardiac delayed rectifier K^+ channel. Role of S6 in antiarrhythmic drug binding. *Circ. Res.* 78:1105–1114.

Yu, S.P., and G.A. Kerchner. 1998. Endogenous voltage-gated potassium channels in human embryonic kidney (HEK293) cells. *J. Neurosci. Res.* 52:612–617.